Abstracta

Ano XXIV - N. 04

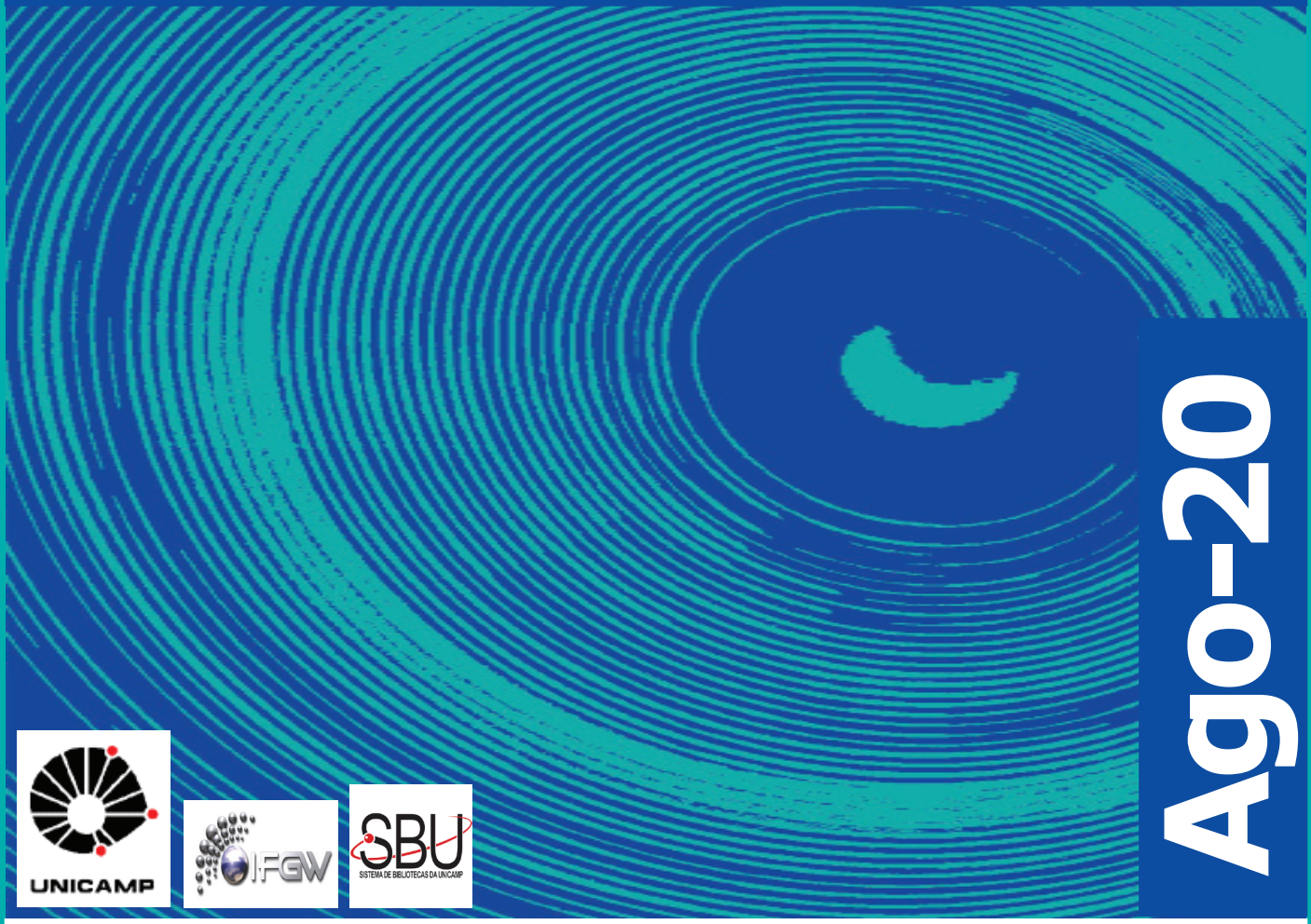

Ago-20

Artigos publicados

[P145-2020] "3D Printing Technology for Tapered Optical Fiber Protection With Gas Sensing Possibilities"

Souza, K. R. de*; Osorio, J. H.*; Carvalho, J. B.*; Lima, B. M.*; Cordeiro, C. M. B.*

We present a new procedure for protecting micro-optical fibers (tapered fibers) by using the 3-dimension (3D) printing technology. A standard single-mode optical fiber was tapered down to the diameter of 1 mu m and embedded in a polymeric matrix obtained by an additive manufacturing routine. We show that the proposed structure protects the fiber taper against environmental humidity while keeping permeability to gas flow and the possibility of the realization of gas detection experiments. To our knowledge, this is the first time 3D printed casings were applied to protect fiber tapers from humidity deterioration. We envisage this new approach will allow the development of new fiber taper devices to better resist in humid environments.

PHOTONIC SENSORS, Jun, 2020. DOI: 10.1007/s13320-020-0592-3

[P146-2020] "A 3-Year Sample of Almost 1,600 Elves Recorded Above South America by the Pierre Auger Cosmic-Ray Observatory"

Aab, A.; Abreu, P.; Aglietta, M.; **Chinellato, J. A.*; Daniel, B.*; Diaz Castro, M. L.*; Dobrigkeit, C.*; Fauth, A. C.*; Muller, M. A.*; Pereira, L. A. S.***; et al.

Elves are a class of transient luminous events, with a radial extent typically greater than 250km, that occur in the lower ionosphere above strong electrical storms. We report the observation of 1,598 elves, from 2014 to 2016, recorded with unprecedented time resolution (100 ns) using the fluorescence detector (FD) of the Pierre Auger Cosmic-Ray Observatory. The Auger Observatory is located in the Mendoza province of Argentina with a viewing footprint for elve observations of 3106km 2, reaching areas above the Pacific and Atlantic Oceans, as well as the Cordoba region, which is known for severe convective thunderstorms. Primarily designed for ultrahigh energy cosmic-ray observations, the Auger FD turns out to be very sensitive to the ultraviolet emission in elves. The detector features modified Schmidt optics with large apertures resulting in a field of view that spans the horizon, and year-round operation on dark nights with low moonlight background, when the local weather is favorable. The measured light profiles of 18% of the elve events have more than one peak, compatible with intracloud activity. Within the 3-year sample, 72% of the elves correlate with the far-field radiation measurements of the World Wide Lightning Location Network. The Auger Observatory plans to continue operations until at least 2025, including elve observations and analysis. To the best of our knowledge, this observatory is the only facility on Earth that measures elves with year-round operation and full horizon coverage.

EARTH AND SPACE SCIENCE 7[4], UNSP e2019EA000582, 2020. DOI: 10.1029/2019EA000582

[P147-2020] "A measurement of the Higgs boson mass in the diphoton decay channel"

Sirunyan, A. M.; Tumasyan, A.; Adam, W.; **Chinellato, J. A.*; Tonelli Manganote, E. J.***; et. al.; CMS Collaboration

A measurement of the mass of the Higgs boson in the diphoton decay channel is presented. This analysis is based on 35.9 fb(-1) of proton-proton collision data collected during the 2016 LHC running period, with the CMS detector at a centre-of-mass energy of 13 TeV. A refined detector calibration and new analysis techniques have been used to improve the precision of this measurement. The Higgs boson mass is measured to be m(H) = 125.78 +/- 0.26GeV. This is combined with a measurement of m(H) already performed in the H -> ZZ -> 4l decay channel using the same data set, giving m(H) = 125.46 +/- 0.16GeV. This result, when further combined with an earlier measurement of m(H) using data collected in 2011 and 2012 with the CMS detector, gives a value for the Higgs boson mass of m(H) = 125.38 +/- 0.14GeV. This is currently the most precise measurement of the mass of the Higgs boson.

PHYSICS LETTERS B 805, 135425, 2020. DOI: 10.1016/j.physletb.2020.135425

[P148-2020] "A thermodynamic study on phase formation and thermal stability of AlSiTaTiZr high -entropy alloy thin films"

Cemin, F.*; Jimenez, M. J. M.*; Leidens, L. M.; Figueroa, C. A.; **Alvarez, F.***

The vast, unexplored chemical realm of multi-principal element alloys (MPEAs) has encouraged researchers to design and synthetize advanced materials based on refractory metals, metalloids, and deoxidizer elements, that are expected to follow single-phase, solid solution high-entropy alloys (HEAs)' footsteps. In this paper, we have theoretically and experimentally studied the AlSiTaTiZr alloy in the thin film form, due to potential applications as a high-temperature oxidation-resistant coating. The MPEA film, synthetized by radio-frequency magnetron sputtering (RFMS), shows a considerable glass-forming ability. However, the metallic glass structure transits to several intermetallic compound phases by post-thermal annealing at ¤873 K, confirming that both thermodynamics and kinetics determine the formation of phases in sputtered MPEAs. Moreover, a strong tendency of Si and Al to form compounds with transition metals was revealed by X-ray diffraction (XRD), X-ray photoelectron spectroscopy (XPS), and thermodynamic investigations. Special focus is given to the role played by both entropy and enthalpy on the phase evolution, demonstrated by thermodynamic calculations using the regular solution model and the CALculation of PHAse Diagrams (CALPHAD) method. This methodology is presented as a useful approach for starting deeper thermodynamic investigations in the thin film literature of MPEAs and HEAs, currently focused on the ultimate properties of such alloys.

JOURNAL OF ALLOYS AND COMPOUNDS 838, 155580, 2020. DOI: 10.1016/j.jallcom.2020.155580

[P149-2020] "Acceleration of Subwavelength Polaritons by Engineering Dielectric-Metallic Substrates"

Feres, F. H.; **Mayer, R. A.***; Barcelos, I. D.; Freitas, R. O.; Maia, F. C. B.

By synchrotron infrared nanospectroscopy, we demonstrate modulation of momentum and group velocity of subdiffractional hyperbolic phonon-polaritons (HP2), in hexagonal boron nitride nanocrystals, by varying the Sio(2) film thickness in the hBN/SiO2/Au heterostructure. We reveal acceleration of the HP2 pulse in a hBN/(SiO2 wedge)/Au heterostructure with gradient of the SiO2 thickness. The acceleration is explained by a semiclassical modeling considering the polariton pulse as a free quantum particle with effective mass dependent on its group velocity. In quantitative agreement with simulations and semiempirical analysis, the modeling predicts an average acceleration of 1.5 x 10(18) m.s(-2) close to that of similar to 1.45 x 10(18) m.s(-2) obtained from experimental inputs. From the fundamental aspect, the polariton acceleration allows discussing the undulatory-corpuscular behavior of polariton quasi-particles. The acceleration induced by the wedge is a general effect that can provide for control of the polariton pulse dynamics, which is compelling for future polaritonic devices.

ACS PHOTONICS 7[6], 1396-1402, 2020. DOI: 10.1021/acsphotonics.0c00563

[P150-2020] "Alginate based nanocomposites with magnetic properties"

Kloster, G. A.; **Muraca, D.*; Londono, O. M.*; Pirota, K. R.***; Mosiewicki, M. A.; Marcovich, N. E.

Superparamagnetic iron oxide nanoparticles (MNP) were synthesized and incorporated into alginate film forming solutions, leading to composite magnetic films. Both plasticized and non-plasticized films were obtained after casting and drying. It was found that part of the MNP are forming agglomerates or clusters of different sizes into the biopolymeric film, while the remaining ones seem to be perfectly dispersed, being the ratio of these arrangements dependent on nanoparticle and glycerol concentrations. We detected that these particles act also as reinforcements when incorporated into non-plasticized matrices, although present the opposite behavior when dispersed into samples containing glycerol. On the other hand, all composite films behave as super-paramagnetic materials, with increasing saturation magnetization as the content of MNP increases and mean blocking temperatures (< T-B >) ranging between 113 and 129 K, which is an expected result due to the strengthening of the dipolar interactions as the size and amount of clusters increase.

COMPOSITES PART A-APPLIED SCIENCE AND MANUFACTURING 135, 105936, 2020. DOI: 10.1016/j.compositesa.2020.105936

[P151-2020] "Allopatry increases the balance of phylogenetic trees during radiation under neutral speciation"

Marquitti, F. M. D.*; Fernandes, L. D.; **Aguiar, M. A. M. de***

The shape of a phylogenetic tree is defined by the sequence of speciation events, represented by its branching points, and extinctions, represented by branch interruptions. In a neutral scenario of parapatry and isolation by distance, species tend to branch off the original population one after the other, leading to highly unbalanced trees. In this case the degree of imbalance, measured by the normalized Sackin index, grows linearly with species richness. Here we claim that moderate values of imbalance for trees with large number of species can occur if the geographic distribution involves more than one deme (allopatry) and speciation is parapatric within demes. The combined values of balance (normalized Sackin index) and species richness provide an estimate of how many demes were involved in the process if it happened in such neutral scenario. We also show that the spatial division in demes moderately slows down the diversification process, portraying a neutral mechanism for structuring the branch length distribution of phylogenetic trees.

ECOGRAPHY 04937, Jul, 2020. DOI: 10.1111/ecog.04937

[P152-2020] "Boosting Electrical Conductivity of Sugarcane Cellulose and Lignin Biocarbons through Annealing under Isopropanol Vapor"

Fingolo, A. C.; Bettini, J.; Cavalcante, M. da S.; Pereira, M. P.; **Bufon, C. C. B.***; Santhiago, M.; Strauss, M.

Annealing of sugarcane bagasse cellulose or lignin biocarbons under isopropanol vapor has induced an improvement in electrical conductivity of these materials. Remarkably, the sheet resistance dropped nearly three times for lignin biocarbon treated with isopropanol vapors. The use of isopropanol vapor annealing has increased sp(2) carbon and decreased oxygenated functionality contents of these biocarbons. These chemical changes were confirmed by X-ray photoelectron and Raman spectroscopy analyses. Transmission electron microscopy images revealed the formation of graphitic domains on samples pyrolyzed in the presence of isopropanol, while electron energy loss spectroscopy mapping at a nanoscale showed an increase in graphitic characteristics of the particles. These chemical and structural changes of biocarbons have improved their electrical conductivity and decreased sheet resistance values of conductive tracks prepared with such materials. As a proof of concept, we fabricated flexible electronic circuits and paper-based electrochemical devices using conductive lignin-based inks prepared with our method.

ACS SUSTAINABLE CHEMISTRY & ENGINEERING 8[18], 7002-7010, 2020. DOI: 10.1021/acssuschemeng.0c00320

[P153-2020] "Bosonic topological insulator intermediate state in the superconductor-insulator transition"

Diamantini, M. C.; Mironov, A. Yu; Postolova, S., V; Liu, X.; Hao, Z.; Silevitch, D. M.; **Kopelevich, Y.***; Kim, P.; Trugenberger, C. A.; Vinokur, V. M.

A low-temperature intervening metallic regime arising in the two-dimensional superconductor-insulator transition challenges our understanding of electronic fluids. Here we develop a gauge theory revealing that this emergent anomalous metal is a bosonic topological insulator where bulk transport is suppressed by mutual statistics interactions between out-of-condensate Cooper pairs and vortices and the longitudinal conductivity is mediated by symmetry-protected gapless edge modes. We explore the magnetic-field-driven superconductor-insulator transition in a niobium titanium nitride device and find marked signatures of a bosonic topological insulator behavior of the intervening regime with the saturating resistance. The observed superconductor-anomalous metal and insulator-anomalous metal dual phase transitions exhibit quantum Berezinskii-Kosterlitz-Thouless criticality in accord with the gauge theory.

PHYSICS LETTERS A 384[23], 126570, 2020. DOI: 10.1016/j.physleta.2020.126570

[P154-2020] "Calibration of the CMS hadron calorimeters using proton-proton collision data at root s=13 TeV"

Sirunyan, A. M.; Tumasyan, A.; Adam, W.; **Chinellato, J. A.*; Tonelli Manganote, E. J.***; et. al.; CMS Collaboration

Methods are presented for calibrating the hadron calorimeter system of theCMSetector at the LHC. The hadron calorimeters of the CMS experiment are sampling calorimeters of brass and scintillator, and are in the form of one central detector and two endcaps. These calorimeters cover pseudorapidities vertical bar eta vertical bar < 3 and are positioned inside the solenoidal magnet. An outer calorimeter, outside the magnet coil, covers vertical bar eta vertical bar < 1.26, and a steel and quartz-fiber Cherenkov forward calorimeter extends the coverage to vertical bar eta vertical bar < 5.19. The initial calibration of the calorimeters was based on results from test beams, augmented with the use of radioactive sources and lasers. The calibration was improved substantially using proton-proton collision data collected at root s = 7, 8, and 13 TeV, as well as cosmic ray muon data collected during the periods when the LHC beams were not present. The present calibration is performed using the 13 TeV data collected during 2016 corresponding to an integrated luminosity of 35.9 fb(-1). The intercalibration of channels exploits the approximate uniformity of energy collection over the azimuthal angle. The absolute energy scale of the central and endcap calorimeters is set using isolated charged hadrons. The energy scale for the electromagnetic portion of the forward calorimeters is set using Z -> ee data.

The energy scale of the outer calorimeters has been determined with test beam data and is confirmed through data with high transverse momentum jets. In this paper, we present the details of the calibration methods and accuracy.

JOURNAL OF INSTRUMENTATION 15[5], P05002, 2020. DOI: 10.1088/1748-0221/15/05/P05002

[P155-2020] "Centrality and transverse momentum dependence of inclusive J/psi production at midrapidity in Pb-Pb collisions at root s NN=5 .02 TeV"

Acharya, S.; Adamova, D.; Adler, A.; **Albuquerque, D. S. D.*; Chinellato, D. D.*; Takahashi, J.***; et. al.; ALICE Collaboration

The shaping of group velocity dispersion in microresonators is an important component in the generation of wideband optical frequency combs. Small resonators-with tight bending radii-offer the large free-spectral range desirable for wide comb formation. However, the tighter bending usually limits comb formation as it enhances normal group velocity dispersion. We experimentally demonstrate that engineering the sidewall angle of a small-radius (▫100μm), 3-μm-thick silica wedge microdisk enables dispersion tuning in both normal and anomalous regimes, without significantly affecting the free spectral range. A microdisk with a wedge angle of 55° (anomalous dispersion) is used to demonstrate a 300 nm bandwidth Kerr optical frequency comb.

PHYSICS LETTERS B 805, 135434, 2020. DOI: 10.1016/j.physletb.2020.135434

[P156-2020] "Channel capacity in brain-computer interfaces"

Costa, T. B. da S.; Uribe, L. F. S.; Carvalho, S. N. de; Soriano, D. C.; **Castellano, G.***; Suyama, R.; Attux, R.; Panazio, C.

Objective. Adapted from the concept of channel capacity, the information transfer rate (ITR) has been widely used to evaluate the performance of a brain-computer interface (BCI). However, its traditional formula considers the model of a discrete memoryless channel in which the transition matrix presents very particular symmetries. As an alternative to compute the ITR, this work indicates a more general closed-form expression-also based on that channel model, but with less restrictive assumptions-and, with the aid of a selection heuristic based on a wrapper algorithm, extends such formula to detect classes that deteriorate the operation of a BCI system. Approach. The benchmark is a steady-state visually evoked potential (SSVEP)--based BCI dataset with 40 frequencies/classes, in which two scenarios are tested: (1) our proposed formula is used and the classes are gradually evaluated in the order of the class labels provided with the dataset; and (2) the same formula is used but with the classes evaluated progressively by a wrapper algorithm. In both scenarios, the canonical correlation analysis (CCA) is the tool to detect SSVEPs. Main results. Before and after class selection using this alternative ITR, the average capacity among all subjects goes from 3.71 +/- 1.68 to 4.79 +/- 0.70 bits per symbol, with p-value<0.01, and, for a supposedly BCI--illiterate subject, her/his capacity goes from 1.53 to 3.90 bits per symbol. Significance. Besides indicating a consistent formula to compute ITR, this work provides an efficient method to perform channel assessment in the context of a BCI experiment and argues that such method can be used to study BCI illiteracy.

JOURNAL OF NEURAL ENGINEERING 17[1], 016060, 2020. DOI: 10.1088/1741-2552/ab6cb7

[P157-2020] "Coherent photoproduction of rho(0) vector mesons in ultra-peripheral Pb-Pb collisions at root s(NN)=5.02 TeV"

Acharya, S.; Adamova, D.; Adler, A.; **Albuquerque, D. S. D.*; Chinellato, D. D.*; Takahashi, J.***; et. al.; ALICE Collaboration

Cross sections for the coherent photoproduction of rho(0) vector mesons in ultra-peripheral Pb-Pb collisions at root s(NN) = 5.02 TeV are reported. The measurements, which rely on the pi(+)pi(-) decay channel, are presented in three regions of rapidity covering the range vertical bar y vertical bar < 0.8. For each rapidity interval, cross sections are shown for different nuclear-breakup classes defined according to the presence of neutrons measured in the zero-degree calorimeters. The results are compared with predictions based on different models of nuclear shadowing. Finally, the observation of a coherently produced resonance-like structure with a mass around 1.7 GeV/c(2) and a width of about 140 MeV/c(2) is reported and compared with similar observations from other experiments.

JOURNAL OF HIGH ENERGY PHYSICS 6, 35, 2020. DOI: 10.1007/JHEP06(2020)035

[P158-2020] "Construction of precision wire readout planes for the Short-Baseline Near Detector (SBND)"

Acciarri, R.; Adams, C.; Andreopoulos, C.; **Bazetto, M. C. Q.*; de Souza, G.*; Gatti, H. F.*; Kemp, E.*; Machado, A. A.*; Peres, O. L. G.***; **Peres, O.*; Pimentel, V. L.*; Segreto, E.*; Soares, R.*; Souza, H. V.*; Stenico, G. V.***; et. al.; SBND Collaboration

The Short-Baseline Near Detector time projection chamber is unique in the design of its charge readout planes. These anode plane assemblies (APAs) have been fabricated and assembled to meet strict accuracy and precision requirements: wire spacing of 3 mm +/- 0.5 mm and wire tension of 7 N +/- 1 N across 3,964 wires per APA, and flatness within 0.5 mm over the 4 m x 2.5 m extent of each APA. This paper describes the design, manufacture and assembly of these key detector components, with a focus on the quality assurance at each stage.

JOURNAL OF INSTRUMENTATION 15[6], P06033, 2020. DOI: 10.1088/1748-0221/15/06/P06033

[P159-2020] "Cosmic-Ray Anisotropies in Right Ascension Measured by the Pierre Auger Observatory"

Aab, A.; Abreu, P.; Aglietta, M.; **Chinellato, J. A.*; de Oliveira Franco, D.*; Diaz Castro, M. L.*; Dobrigkeit, C.*; Fauth, A. C*.; Payeras, A. M.*; Muller, M. A.*; Pereira, L. A. S.*;** et. al.; Pierre Auger Collaboration

We present measurements of the large-scale cosmic-ray (CR) anisotropies in R.A., using data collected by the surface detector array of the Pierre Auger Observatory over more than 14 yr. We determine the equatorial dipole component, d(perpendicular to), through a Fourier analysis in R.A. that includes weights for each event so as to account for the main detector-induced systematic effects. For the energies at which the trigger efficiency of the array is small, the "east-west" method is employed. Besides using the data from the array with detectors separated by 1500.m, we also include data from the smaller but denser subarray of detectors with 750 m separation, which allows us to extend the analysis down to similar to 0.03.EeV. The most significant equatorial dipole amplitude obtained is that in the cumulative bin above 8.EeV, = d(perpendicular to) = 6.0(-0.9) (+1.0)%, which is inconsistent with isotropy at the 6 sigma level. In the bins below 8.EeV, we obtain 99% CL upper bounds on d(perpendicular to) at the level of 1%-3%. At energies below 1.EeV, even though the amplitudes are not significant, the phases determined in most of the bins are not far from the R.A. of the Galactic center, at (GC)=-94 degrees, suggesting a predominantly Galactic origin for anisotropies at these energies.

The reconstructed dipole phases in the energy bins above 4.EeV point instead to R.A. that are almost opposite to the Galactic center one, indicative of an extragalactic CR origin.alpha

ASTROPHYSICAL JOURNAL 891[2], 142, 2020. DOI: 10.3847/1538-4357/ab7236

[P160-2020] "Dark Energy Survey Year 1 Results: Wide-field mass maps via forward fitting in harmonic space"

Mawdsley, B.; Bacon, D.; Chang, C.; **Sobreira, F.***; et. al.; DES Collaboration

We present new wide-field weak lensing mass maps for the Year 1 Dark Energy Survey (DES) data, generated via a forward fitting approach. This method of producing maps does not impose any prior constraints on the mass distribution to be reconstructed. The technique is found to improve the map reconstruction on the edges of the field compared to the conventional Kaiser--Squires method, which applies a direct inversion on the data; our approach is in good agreement with the previous direct approach in the central regions of the footprint. The mapping technique is assessed and verified with tests on simulations; together with the Kaiser-Squires method, the technique is then applied to data from the DES Year 1 data and the differences between the two methods are compared. We also produce the first DES measurements of the convergence Minkowski functionals and compare them to those measured in simulations.

MONTHLY NOTICES OF THE ROYAL ASTRONOMICAL SOCIETY 493[4], 5662-5679, 2020. DOI: 10.1093/mnras/staa565

[P161-2020] "Determination of the strong coupling constant alpha(S)(m(Z)) from measurements of inclusive W-+/- and Z boson production cross sections in proton-proton collisions at root s=7 and 8 TeV"

Sirunyan, A. M.; Tumasyan, A.; Adam, W.; Chinellato, J. A.*; Tonelli Manganote, E. J.*; et. al.; CMS Collaboration

Twelve measurements of inclusive cross sections of W-+/- and Z boson production, performed in proton-proton collisions at centre-of-mass energies of 7 and 8 TeV, are compared with perturbative quantum chromodynamics calculations at next--to-next- to-leading order (NNLO) accuracy obtained with the CT14, HERAPDF2.0, MMHT14, and NNPDF3.0 parton distribution functions (PDFs). Data and theory agree well for all PDF sets, taking into account the experimental and theoretical uncertainties. A novel procedure is employed to extract the strong coupling constant at the Z pole mass from a detailed comparison of all the experimental fiducial cross sections to the corresponding NNLO theoretical predictions, yielding alpha S (m(Z)) = 0.1163(-0.0031)(+0.0024) (CT14), 0.1072(-0.0040)(+0.0043) (HERAPDF2.0), 0.1186 +/- 0. 0025 (MMHT14), and 0.1147 +/- 0.0023 (NNPDF3.0). Using the results obtained with the CT14 and MMHT14 PDFs, which yield the most robust and stable alpha(S)(mZ) extractions, a value alpha(S)(m(Z)) = 0.1175(-0.0028)(+0.0025) is determined.

JOURNAL OF HIGH ENERGY PHYSICS 6, 18, 2020. DOI: 10.1007/JHEP06(2020)018

[P162-2020] "Dispersion tailoring in wedge microcavities for Kerr comb generation"

Fujii, L.*; Inga, M.*; Soares, J. H.*; Espinel, Y. A., V*; Mayer Alegre, T. P.*; Wiederhecker, G. S.*

The shaping of group velocity dispersion in microresonators is an important component in the generation of wideband optical frequency combs. Small resonators-with tight bending radii-offer the large free-spectral range desirable for wide comb formation. However, the tighter bending usually limits comb formation as it enhances normal group velocity dispersion. We experimentally demonstrate that engineering the sidewall angle of a small-radius (similar to 100 mu m), 3-mu m-thick silica wedge microdisk enables dispersion tuning in both normal and anomalous regimes, without significantly affecting the free spectral range. A microdisk with a wedge angle of 55 degrees (anomalous dispersion) is used to demonstrate a 300 nm bandwidth Kerr optical frequency comb.

OPTICS LETTERS 45[12], 3232-3235, 2020. DOI: 10.1364/OL.393294

[P163-2020] "Effect of deposition angle on fabrication of plasmonic gold nanocones and nanodiscs"

Liska, J.; Ligmajer, F.; **Pinho, P. V. N.*;** Kejik, L.; Kvapil, M.; Dvorak, P.; Horky, M.; Leitner, N. S.; Reimhult, E.; Sikola, T.

Metal nanocones can exhibit several strong plasmonic resonances, which are associated with intense and accessible electromagnetic hot spots. They can thus be used to enhance light--matter interactions or to facilitate location-specific sensing while enabling separation of some non-specific contributions towards the sensing signal. Nanocones and similar 3D structures are often fabricated with the use of the so-called self-shading effect, which occurs during the evaporation of a metal film into circular nanowells. Unfortunately, a full description of a successful deposition process with all the essential details is currently missing in literature. Here we present a detailed view of the fabrication of ordered arrays of conical gold nanostructures using electron beam lithography and gold electron beam evaporation. We show that the symmetry of the fabricated nanostructures is influenced by the lateral position of the substrate on the sample holder during the deposition. Off--axis deposition or tilt of the sample leads to asymmetric nanostructures. When the deposited film is thick enough, or the nanowells narrow enough, the entrance aperture is clogged, and nanocones with sharp tips are formed. In contrast, flat--top truncated cones are produced for thinner films or wider nanowells. All these findings help to identify inherent limits for the production of wafer-scale arrays of such non-planar nanostructures. On the other hand, they also suggest new fabrication possibilities for more complicated structures such as mutually connected nanocones for electrically addressable chips.

MICROELECTRONIC ENGINEERING 228, 111326, 2020. DOI: 10.1016/j.mee.2020.111326

[P164-2020] "Effective killing of bacteria under blue-light irradiation promoted by green synthesized silver nanoparticles loaded on reduced graphene oxide sheets"

Caires, C. S. A.; Farias, L. A. S.; Gomes, L. E.; Pinto, B. P.; Goncalves, D. A.; **Zagonel, L. F.***; Nascimento, V. A.; Alves, D. C. B.; Colbeck, I.; Whitby, C.; Caires, A. R. L.; Wender, H.

Graphene oxide (GO) materials loaded with silver nanoparticles (AgNPs) have drawn considerable attention due to their capacity to efficiently inactivate bacteria though a multifaceted mechanism of action, as well as for presenting a synergetic effect against bacteria when compared to the activity of AgNPs and GO alone. In this investigation, we present an inexpensive and environmentally-friendly method for synthesizing reduced GO sheets coated with silver nanoparticles (AgNPs/rGO) using a coffee extract solution as a green reducing agent.

The physical and chemical properties of the produced materials were extensively characterized by scanning electron microscopy (SEM), field-emission gun transmission electron microscopy (FEG-TEM), ultraviolet and visible absorption (UV-Vis), Raman spectroscopy, X-ray photoelectron spectroscopy (XPS), inductively coupled plasma-optical emission spectroscopy (ICP-OES) and ion release determination. The results demonstrated that AgNPs/r-GO composites were successfully produced, revealing the formation of micrometer-sized r-GO sheets decorated by AgNPs of approximately 70 nm diameter. Finally, bactericidal and photobactericidal effects of the AgNPs/r-GO composites were tested against Staphylococcus aureus, in which the results showed that the composites presented antimicrobial and photoantimicrobial activities. Moreover, our results demonstrated for the first time, to our knowledge, that an efficient process of bacterial inactivation can be achieved by using AgNPs/r-GO composites under blue light irradiation as a result of three different bacterial killing processes: (i) chemical effect promoted by Ag+ ion release from AgNPs; (ii) photocatalytic activity induced by AgNPs/r-GO composites, enhancing the bacterial photoinactivation due to the excited-Plasmons of the AgNPs when anchored on r-GO; and (iii) photodynamic effect produced by bacterial endogenous photosensitizers under blue-light irradiation. In summary, the present findings demonstrated that AgNPs/r-GO can be obtained by a non-toxic procedure with great potential for biomedical-related applications.

MATERIALS SCIENCE & ENGINEERING C-MATERIALS FOR BIOLOGICAL APPLICATIONS 113, 110984, 2020. DOI: 10.1016/j.msec.2020.110984

[P165-2020] "Electronic and magnetic properties of stoichiometric CeAuBi2"

Piva, M. M.*; Tartaglia, R.*; Freitas, G. S.*; Souza, J. C.*; Christovam, D. S.*; Thomas, S. M.; Leao, J. B.; Ratcliff, W.; Lynn, J. W.; Lane, C.; Zhu, J-X; Thompson, J. D.; Rosa, P. F. S.; **Adriano, C.*; Granado, E.*; Pagliuso, P. G.***

We report the electronic and magnetic properties of stoichiometric CeAuBi2 single crystals. At ambient pressure, CeAuBi2 orders antiferromagnetically below a Neel temperature (T-N) of 19 K. Neutron diffraction experiments revealed an antiferromagnetic propagation vector (tau) over cap = [0, 0, 1/2], which doubles the paramagnetic unit cell along the c axis. At low temperatures several metamagnetic transitions are induced by the application of fields parallel to the c axis, suggesting that the magnetic structure of CeAuBi2 changes as a function of field. At low temperatures, a linear positive magnetoresistance may indicate the presence of band crossings near the Fermi level. Finally, the application of external pressure favors the antiferromagnetic state, indicating that the 4f electrons become more localized.

PHYSICAL REVIEW B 101[21], 214431, 2020. DOI: 10.1103/PhysRevB.101.214431

[P166-2020] "Electronic excitation of ethanol by low-energy electron impact"

Falkowski, A. G.*; Lima, M. A. P.*; Kossoski, F.*

We report computed differential cross sections (DCSs) for electron impact excitation of the lower-lying states of both trans and gauche tautomers of ethanol, as well as total cross sections for the 15 eV-50 eV energy range. The Schwinger multichannel (SMC) method with pseudopotentials has been employed, and in our most sophisticated calculation in terms of multichannel coupling, 431 open target states have been considered. We found an overall good agreement with the available experimental data at intermediate scattering angles and at higher impact energies. Although we have used a Born-closure scheme for the higher partial waves, we have found discrepancies in the forward direction that were assigned to a poor description of the long-range component of the lower partial waves. Meanwhile, the lack of more Rydberg states could be related to the overestimated DCSs at lower energies. Missing open channels are usually evoked to explain the remaining discrepancies to experiment, but here, we argue that other factors should also be involved. Aiming at an improved description of the target states, we have proposed a simple procedure for selecting the pairs of hole and particle orbitals while keeping the single excitation prescription of the current SMC implementation. A quantitative assessment of the collision process should further consider the individual contribution of each tautomer, which presented quite distinct DCSs in some cases. Our computed excitation energies also support that the second absorption band of ethanol is comprised of three singlet states of each tautomer, rather than the previously suggested two or four states.

JOURNAL OF CHEMICAL PHYSICS 152[24], 244302, 2020. DOI: 10.1063/5.0008428

[P167-2020] "Estimation of glandular dose in mammography based on artificial neural networks"

Massera, R. T.*; Tomal, A.*

This work proposes using artificial neural networks (ANNs) for the regression of the dosimetric quantities employed in mammography. The data were generated by Monte Carlo (MC) simulations using a modified and validated version of the PENELOPE (v. 2014) + penEasy (v. 2015) code. A breast model of a homogeneous mixture of adipose and glandular tissue was adopted. The ANNs were constructed using the Keras and scikit-learn libraries for mean glandular dose (MGD) and air kerma (K-air) regressions, respectively. In total, seven parameters were considered, including the incident photon energies (from 8.25 to 48.75 keV), breast geometry, breast glandularity and K-air acquisition geometry. Two ensembles of five ANNs each were formed to calculate MGD and K-air. The normalized glandular dose coefficients (DgN) were calculated using the ratio of the ensemble outputs for MGD and K-air. Polyenergetic DgN values were calculated by weighting monoenergetic values by the spectrum bin probabilities. The results indicate a very good ANN prediction performance when compared to the validation data, with median errors on the order of the average simulation uncertainties (& x224d; 0.2%). Moreover, the predicted DgN values are in good agreement compared with previously published works, with mean (maximum) differences up to 2.2% (9.4%). Therefore, it is shown that ANNs could be a complementary or alternative technique to tables, parametric equations and polynomial fits to estimate DgN values obtained via MC simulations.

PHYSICS IN MEDICINE AND BIOLOGY 65[9], 095009, 2020. DOI: 10.1088/1361-6560/ab7a6d

[P168-2020] "Evidence of Spin-Orbital Angular Momentum Interactions in Relativistic Heavy-Ion Collisions"

Acharya, S.; Adamova, D.; Adler, A.; **Albuquerque, D. S. D.*; Chinellato, D. D.*; Takahashi, J.***; et. al.; ALICE Collaboration

The first evidence of spin alignment of vector mesons (K*(0) and phi) in heavy-ion collisions at the Large Hadron Collider (LHC) is reported. The spin density matrix element rho(00) is measured at midrapidity (vertical bar y vertical bar < 0.5) in Pb-Pb collisions at a center-of-mass energy root(s)NNof 2.76 TeV with the ALICE detector. rho(00) values are found to be less than 1/3 (1/3 implies no spin alignment) at low transverse momentum (p(T) < 2 GeV / c) for K*(0) and phi at a level of 3 sigma and 2 sigma, respectively.

No significant spin alignment is observed for the K-S(0) meson (spin = 0) in Pb-Pb collisions and for the vector mesons in pp collisions. The measured spin alignment is unexpectedly large but qualitatively consistent with the expectation from models which attribute it to a polarization of quarks in the presence of angular momentum in heavy-ion collisions and a subsequent hadronization by the process of recombination.

PHYSICAL REVIEW LETTERS 125[1], 012301, 2020. DOI: 10.1103/PhysRevLett.125.012301

[P169-2020] "Experimental study of different silicon sensor options for the upgrade of the CMS Outer Tracker"

Sirunyan, A. M.; Tumasyan, A.; Adam, W.; **Chinellato, J. A.*; Tonelli Manganote, E. J.***; et. al.; CMS Collaboration

During the high-luminosity phase of the LHC (HL-LHC), planned to start in 2027, the accelerator is expected to deliver an instantaneous peak luminosity of up to 7.5 x 10(34) cm(-2) s(-1). A total integrated luminosity of 3000 or even 4000 fb(-1) is foreseen to be delivered to the general purpose detectors ATLAS and CMS over a decade, thereby increasing the discovery potential of the LHC experiments significantly. The CMS detector will undergo a major upgrade for the HL-LHC, with entirely new tracking detectors consisting of an Outer Tracker and Inner Tracker. However, the new tracking system will be exposed to a significantly higher radiation than the current tracker, requiring new radiation-hard sensors. CMS initiated an extensive irradiation and measurement campaign starting in 2009 to systematically compare the properties of different silicon materials and design choices for the Outer Tracker sensors. Several test structures and sensors were designed and implemented on 18 different combinations of wafer materials, thicknesses, and production technologies. The devices were electrically characterized before and after irradiation with neutrons, and with protons of different energies, with fluences corresponding to those expected at different radii of the CMS Outer Tracker after 3000 fb(-1). The tests performed include studies with beta sources, lasers, and beam scans. This paper compares the performance of different options for the HL-LHC silicon sensors with a focus on silicon bulk material and thickness.

JOURNAL OF INSTRUMENTATION 15[4], P04017, 2020. DOI: 10.1088/1748-0221/15/04/P04017

[P170-2020] "Experimental Study on Glass and Polymers: Determining the Optimal Material for Potential Use in Terahertz Technology"

Islam, M. S.; **Cordeiro, C. M. B.***; Nine, M. J.; Sultana, J.; Cruz, A. L. S.; Dinovitser, A.; Ng, B. W. H.; Ebendorff-Heidepriem, H.; Losic, D.; Abbott, D.

The optical properties of polymers and glasses useful for terahertz applications are experimentally characterized using terahertz time-domain spectroscopy (THz-TDS). A standard system setup utilizing transmission spectroscopy is used to measure different optical properties of materials including refractive index, relative permittivity, loss tangent, absorption coefficient, and transmittance. The thermal and chemical dependencies of materials are also studied to identify the appropriate materials for given terahertz applications. The selected materials can then be utilized for applications such as in waveguides, filters, lenses, polarization preserving devices, metamaterials and metasurfaces, absorbers, and sensors in the terahertz frequency range.

IEEE ACCESS 8, 97204-97214, 2020. DOI: 10.1109/ACCESS.2020.2996278

[P171-2020] "Exploring Low Loss and Single Mode in Antiresonant Tube Lattice Terahertz Fibers"

Sultana, J.; Islam, M. S.; **Cordeiro, C. M. B.***; Habib, M. S.; Dinovitser, A.; Ng, B. W. H.; Abbott, D.

We propose and numerically analyze various hollow-core antiresonant fiber (HC-ARF) for operation at terahertz frequencies. We compare typical HC-ARF designs with nested and adjacent nested designs while analyzing performance in terms of loss and single-mode guidance of terahertz waves. With optimized fiber dimensions, the fundamental core mode, cladding mode, core higher-order modes (HOMs), and the angle dependence of adjacent tubes are analyzed to find the best design for low loss terahertz transmission. Analysis of the fiber designs shows that the nested tube-based antiresonant fiber exhibits lower transmission loss and superior HOM suppression, exceeding 140. The nested HC-ARF is feasible for fabrication using existing fabrication technologies and opening up the possibility of efficient transmission of terahertz waves.

IEEE ACCESS 8, 113309-113317, 2020. DOI: 10.1109/ACCESS.2020.3003035

[P172-2020] "Extraction of Two-Dimensional Aluminum Alloys from Decagonal Quasicrystals"

Yadav, T. P.; Woellner, C. F.; Sharifi, T.; Sinha, S. K.; Qu, L.; Apte, A.; Mukhopadhyay, N. K.; Srivastava, O. N.; Vajtai, R.; **Galvao, D. S.***; Tiwary, C. S.; Ajayan, P. M.

Atomically thin metallic alloys are receiving increased attention due to their prospective applications as interconnects/contacts in two-dimensional (2D) circuits, sensors, and catalysts, among others. In this work, we demonstrate an easily scalable technique for the synthesis of 2D metallic alloys from their 3D quasicrystalline precursors. We have used aluminum (Al)-based single-phase decagonal quasicrystal Al66Co17Cu17 alloy to extract the corresponding 2D alloy structure. The 2D layered Al alloy possesses 2-fold decagonal quasicrystalline symmetry and consists of two- or three-layer-thick sheets with a lateral dimension of microns. These 2D metallic layers were combined with the atomic layers of tungsten disulfide to form the stacked heterostructures, which is demonstrated to be a stable and efficient catalyst for hydrogen evolution reaction.

ACS NANO 14[6], 7435-7443, 2020. DOI: 10.1021/acsnano.0c03081

[P173-2020] "First liquid argon test of the X-ARAPUCA"

Segreto, E.*; Machado, A. A.*; Fauth, A.*; Ramos, R. R.*; De Souza, G.*; Souza, H. V.*; Pimentel, V. L.; Bazetto, M. C. Q.; Ayala-Torres, M. A.

The X-ARAPUCA is a device for the detection of scintillation light in liquid argon and represents an evolution of the ARAPUCA design, with an increased collection efficiency and a simpler design. The first liquid argon test of an X--ARAPUCA prototype has been performed in the cryogenic facility of the Laboratorio de Leptons da UNCIAMP and showed a detection efficiency of 3.5% +/- 0.5%, in line with the expectations from Monte Carlo simulations and extrapolations from measurements with standard ARAPUCAs.

JOURNAL OF INSTRUMENTATION 15[5], C05045, 2020. DOI: 10.1088/1748-0221/15/05/C05045

[P174-2020] "First order reversal curve Hall analysis of zero-field skyrmions on Pt/Co/Ta multilayers"

Toneto, D.; Silva, R. B. da; Dorneles, L. S.; **Beron, F.***; Oyarzun, S.; Denardin, J. C.

Magnetic skyrmions are non-trivial spin textures that resist external disturbances and are promising candidates for use in next generation spintronic devices. However, a major challenge in the realization of devices based on skyrmions is the stabilization of ordered arrangements of these spin textures under ambient temperature and zero applied field conditions. Multilayers of ferromagnetic materials (Co) interspersed with heavy metals with strong spin-orbit coupling (Pt and Ta), exhibit interesting properties, as the Dzyaloshinskii-Moriya interaction, which is an anti-symmetric exchange interaction that tilts the spins of neighboring layers, helps to stabilize skyrmions. In this work we study the formation and stabilization of magnetic skyrmions in Pt/Co/Ta films using a first order reversal curve (FORC) analysis, obtained from Hall effect measurements. The analysis of the FORC Hall diagrams was used to determine the intensity of the magnetic fields that should be applied to nucleate and stabilize skyrmions at remanence. Magnetic force microscopy images and micromagnetic simulations were compared to determine the correlation of the domain textures with the applied field and magnetic parameters of the multilayers.

JOURNAL OF PHYSICS D-APPLIED PHYSICS 53[39], 395001, 2020. DOI: 10.1088/1361-6463/ab95be

[P175-2020] "Higher harmonic non-linear flow modes of charged hadrons in Pb-Pb collisions at root s(NN)=5.02 TeV"

Acharya, S.; Adamova, D.; Adler, A.; **Albuquerque, D. S. D.*; Chinellato, D. D.*; Takahashi, J.***; et. al.; ALICE Collaboration

Anisotropic flow coefficients, nu(n), non-linear flow mode coefficients, chi(n,mk), and correlations among different symmetry planes, rho(n,mk) are measured in Pb-Pb collisions at root s(NN) = 5.02TeV. Results obtained with multi-particle correlations are reported for the transverse momentum interval 0.2 < p(T) < 5.0 GeV/c within the pseudorapidity interval 0.4 < vertical bar eta vertical bar < 0.8 as a function of collision centrality. The nu(n) coefficients and chi(n,mk) and rho(n,mk) are presented up to the ninth and seventh harmonic order, respectively. Calculations suggest that the correlations measured in different symmetry planes and the non-linear flow mode coefficients are dependent on the shear and bulk viscosity to entropy ratios of the medium created in heavy-ion collisions. The comparison between these measurements and those at lower energies and calculations from hydrodynamic models places strong constraints on the initial conditions and transport properties of the system.

JOURNAL OF HIGH ENERGY PHYSICS 5, 085, 2020. DOI: 10.1007/JHEP05(2020)085

[P176-2020] "Highly fluorescent few atoms silver nanoclusters with strong photocatalytic activity synthesized by ultrashort light pulses"

Santillan, J. M. J.; Arboleda, D. M.; **Muraca, D.***; Schinca, D.l C.; Scaffardi, L. B.

While there are conventional chemical synthesis methods to generate metal nanoclusters (NCs), many of them are adversely affected by the unavoidable contamination of the nanoproduct solution, resulting in aggregation, background noise in analytical chemistry, toxicity, and deactivation of the catalyst. In this work, physical method of ultrafast laser ablation as a "green" synthesis approach together with mechanical centrifugation to obtain silver NCs, simplifying widely the chemical synthesis requirements, is proposed. Remarkably, compared with conventional methods for synthesizing Ag NCs, this new approach starts with a colloid that contains nanosized particles as well as smaller species, managing to obtain colloids with few atoms NCs by centrifugation. Those colloids were analyzed by fluorescence spectroscopy observing UV bands corresponding with HOMO-LUMO cluster transitions. Besides, independent HRTEM measurements were made confirming the presence of few atoms Ag NCs, as well as small NPs in different formation stages. Equally important, photocatalytic efficiency of the obtained NCs was studied through degradation of Methylene Blue (MB) when it was mixed with as-prepared or highly centrifuged colloid, showing an enhanced photocatalytic efficiency of 79% as compared to 57% for pure MB after 180min of illumination. Consequently, this work contributes to establishing a simple approach to synthesize highly fluorescent and photocatalytic NCs.

SCIENTIFIC REPORTS 10[1], 8217, 2020. DOI: 10.1038/s41598-020-64773-z

[P177-2020] "Identification of heavy, energetic, hadronically decaying particles using machine-learning techniques"

Sirunyan, A. M.; Tumasyan, A.; Adam, W.; **Chinellato, J. A.*; Tonelli Manganote, E. J.***; et. al.; CMS Collaboration

Machine-learning (ML) techniques are explored to identify and classify hadronic decays of highly Lorentz-boosted W/Z/Higgs bosons and top quarks. Techniques without ML have also been evaluated and are included for comparison. The identification performances of a variety of algorithms are characterized in simulated events and directly compared with data. The algorithms are validated using proton-proton collision data at root S = 13 TeV, corresponding to an integrated luminosity of 35.9 fb(-1). Systematic uncertainties are assessed by comparing the results obtained using simulation and collision data. The new techniques studied in this paper provide significant performance improvements over non-ML techniques, reducing the background rate by up to an order of magnitude at the same signal efficiency.

JOURNAL OF INSTRUMENTATION 15[6], P06005, 2020. DOI: 10.1088/1748-0221/15/06/P06005

[P178-2020] "Investigation of the p-Sigma(0) interaction via femtoscopy in pp collisions"

Acharya, S.; Adamova, D.; Adler, A.; **Albuquerque, D. S. D.*; Chinellato, D. D.*; Takahashi, J.***; et. al.; ALICE Collaboration

This Letter presents the first direct investigation of the p--Sigma(0) interaction, using the femtoscopy technique in high--multiplicity pp collisions at root s = 13 TeV measured by the ALICE detector. The Sigma(0) is reconstructed via the decay channel to Lambda gamma, and the subsequent decay of Lambda to p pi(-). The photon is detected via the conversion in material to e(+)e(-) pairs exploiting the capability of the ALICE detector to measure electrons at low transverse momenta. The measured p-Sigma(0) correlation indicates a shallow strong interaction. The comparison of the data to several theoretical predictions obtained employing the Correlation Analysis Tool using the Schrodinger Equation (CATS) and the Lednicky--Lyuboshits approach shows that the current experimental precision does not yet allow to discriminate between different models, as it is the case for the available scattering and hypernuclei data. Nevertheless, the p-Sigma(0) correlation function is found to be sensitive to the strong interaction, and driven by the interplay of the different spin and isospin channels. This pioneering study demonstrates the feasibility of a femtoscopic measurement in the p-Sigma(0) channel and with the expected larger data samples in LHC Run 3 and Run 4, the p-Sigma(0) interaction will be constrained with high precision.

PHYSICS LETTERS B 805, 135419, 2020. DOI: 10.1016/j.physletb.2020.135419

[P179-2020] "Jet-hadron correlations measured relative to the second order event plane in Pb-Pb collisions at root s(NN)=2.76 TeV"

Acharya, S.; Adamova, D.; Adler, A.; **Albuquerque, D. S. D.*; Chinellato, D. D.*; Takahashi, J.***; et. al.; ALICE Collaboration

The quark gluon plasma produced in ultrarelativistic heavy-ion collisions at the Large Hadron Collider (LHC) can be studied by measuring the modifications of jets formed by hard scattered partons which interact with the medium. We studied these modifications via angular correlations of jets with charged hadrons for jets with momenta 20 < P-T(jet)< 40 GeV/c as a function of the associated particle momentum. The reaction plane fit method is used in this analysis to remove the flow modulated background. The analysis of angular correlations for different orientations of the jet relative to the second order event plane allows for the study of the path length dependence of medium modifications to jets. We present the dependence of azimuthal angular correlations of charged hadrons with respect to the angle of the axis of a reconstructed jet relative to the event plane in Pb-Pb collisions at root s(NN) = 2.76 TeV. The dependence of particle yields associated with jets on the angle of the jet with respect to the event plane is presented. Correlations at different angles relative to the event plane are compared through ratios and differences of the yield. No dependence of the results on the angle of the jet with respect to the event plane is observed within uncertainties, which is consistent with no significant path length dependence of the medium modifications for this observable.

PHYSICAL REVIEW C 101[6], 064901, 2020. DOI: 10.1103/PhysRevC.101.064901

[P180-2020] "Longitudinal and azimuthal evolution of two--particle transverse momentum correlations in Pb-Pb collisions at root s(NN)=2.76 TeV"

Acharya, S.; Adamova, D.; Adhya, S. P.; **Albuquerque, D. S. D.*; Chinellato, D. D.*; De Souza, R. D.*; Takahashi, J.***; et. al.; ALICE Collaboration

This paper presents the first measurements of the charge independent (CI) and charge dependent (CD) two-particle transverse momentum correlators G(2)(CI) and G(2)(CD) in Pb-Pb collisions at root sNN= 2.76 TeVby the ALICE collaboration. The two-particle transverse momentum correlator G(2) was introduced as a measure of the momentum current transfer between neighboringsystem cells. The correlators are measured as a function of pair separation in pseudorapidity (Delta eta) and azimuth (Delta phi) and as a function of collision centrality. From peripheral to central collisions, the correlator G(2)(CI) exhibits a longitudinal broadening while undergoing a monotonic azimuthal narrowing. By contrast, G(2)(CD) exhibits a narrowing along both dimensions. These features are not reproduced by models such as HIJING and AMPT. However, the observed narrowing of the correlators from peripheral to central collisions is expected to result from the stronger transverse flow profiles produced in more central collisions and the longitudinal broadening is predicted to be sensitive to momentum currents and the shear viscosity per unit of entropy density./sof the matter produced in the collisions. The observed broadening is found to be consistent with the hypothesized lower bound of eta/s and is in qualitative agreement with values obtained from anisotropic flow measurements.

PHYSICS LETTERS B 804, 135375, 2020. DOI: 10.1016/j.physletb.2020.135375

[P181-2020] "Magnetization of Bi2Sr2CaCu2O8+delta Micrometer Thin Ring and Its Depinning Line"

Semenenko, B.; Camargo, B. C.; Setzer, A.; Boehlmann, W.; **Kopelevich, Y.***; Esquinazi, P. D.

We demonstrate a geometrical effect on the depinning line (DL) of the flux line lattice of the Bi2Sr2CaCu2O8+delta high--T-c superconductor (HTSC) micrometer ring. The DL shifts to notably lower temperatures in comparison with bulk crystals and thin flakes of the same sample. The shift is attributed to a decrease in the overall pinning potential due to a double size effect, namely (a) the ring thickness similar to 1 mu m being smaller than the pinning correlation length and (b) the increase in the effective London penetration depth of the vortices (Pearl vortices). The large shift of the DL to lower temperatures may influence the suitability of this HTSC for applications in microstrip antennas and THz emitters.

JOURNAL OF SUPERCONDUCTIVITY AND NOVEL MAGNETISM, 2020. DOI: 10.1007/s10948-020-05507-0

[P182-2020] "Mean-field theory of interacting triplons in a two-dimensional valence-bond solid: Stability and properties of many-triplon states"

Doretto, R. L.*

We study a system of (N) over bar interacting triplons (the elementary excitations of a valence-bond solid) described by an effective interacting boson model derived within the bond operator formalism in order to determine the stability and the properties of many-triplon states. In particular, we consider the square lattice spin-1/2 J(1)-J(2) antiferromagnetic Heisenberg model, focus on the intermediate parameter region where a quantum paramagnetic phase sets in, and consider the columnar valence-bond solid as a reference state. Within the bond operator theory, the Heisenberg model is mapped into an effective boson model in terms of triplet operators t. The effective boson model is studied at the harmonic approximation and the energy of the triplons and the expansion of the triplon operators b in terms of the triplet operators t are determined. Such an expansion allows us to perform a second mapping and, therefore, determine an effective interacting boson model in terms of the triplon operators b. We then consider systems with a fixed number (N) over bar of triplons and study the stability of many-triplon states within a mean-field approximation. We show that many-triplon states are stable, the lowest-energy ones are constituted by a small number of triplons, and the excitation gaps are finite. For J(2) = 0.48J(1) and 0.52J(1), we also calculate spin-spin and dimer--dimer correlation functions, dimer order parameters, and the bipartite von Neumann entanglement entropy within our mean-field formalism in order to determine the properties of the many-triplon state as a function of the triplon number (N) over bar. We find that the spin and the dimer correlations decay exponentially and that the entanglement entropy obeys an area law, regardless of the triplon number (N) over bar. Moreover, only for J(2) = 0.48J(1), the spin correlations indicate that the many-triplon states with large triplon number (N) over bar might display a more homogeneous singlet pattern than the columnar valence-bond solid. We also comment on possible relations between the many-triplon states with large triplon number (N) over bar and gapped spin-liquid states.

PHYSICAL REVIEW B 102[1], 014415, 2020. DOI: 10.1103/PhysRevB.102.014415

[P183-2020] "Measurement of differential cross sections and charge ratios for t-channel single top quark production in proton-proton collisions at root s = 13 TeV"

Sirunyan, A. M.; Tumasyan, A.; Adam, W.; **Chinellato, J. A.*; Tonelli Manganote, E. J.***; et. al.; CMS Collaboration

A measurement is presented of differential cross sections for t-channel single top quark and antiquark production in proton-proton collisions at a centre-of-mass energy of 13 mml:mspace> by the CMS experiment at the LHC. From a data set corresponding to an integrated luminosity of 35.9 mml:mspacefb-1, events containing one muon or electron and two or three jets are analysed. The cross section is measured as a function of the top quark transverse momentum (pT), rapidity, and polarisation angle, the charged lepton pT and rapidity, and the pT of the W boson from the top quark decay. In addition, the charge ratio is measured differentially as a function of the top quark, charged lepton, and W boson kinematic observables. The results are found to be in agreement with standard model predictions using various next-to--leading-order event generators and sets of parton distribution functions. Additionally, the spin asymmetry, sensitive to the top quark polarisation, is determined from the differential distribution of the polarisation angle at parton level to be 0.440 +/- 0.070, in agreement with the standard model prediction.

EUROPEAN PHYSICAL JOURNAL C 80[5], 370, 2020. DOI: 10.1140/epjc/s10052-020-7858-1

[P184-2020] "Measurement of electrons from semileptonic heavy-flavour hadron decays at midrapidity in pp and Pb-Pb collisions at root s(NN)=5.02 TeV"

Acharya, S.; Adamova, D.; Adhya, S. P.; **Albuquerque, D. S. D.*; Chinellato, D. D.*; De Souza, R. D.*; Takahashi, J.***; et. al.; ALICE Collaboration

The differential invariant yield as a function of transverse momentum (p(T)) of electrons from semileptonic heavy-flavour hadron decays was measured at midrapidity in central (0-10%), semi-central (30-50%) and peripheral (60-80%) lead-lead (Pb-Pb) collisions at root s(NN) = 5.02 TeV in the p(T) intervals 0.5-26GeV/c(0-10% and 30-50%) and 0.5-10 GeV/c (60-80%). The production cross section in proton-proton (pp) collisions at root s = 5.02 TeV was measured as well in 0.5 < pT< 10GeV/c and it lies close to the upper band of perturbative QCD calculation uncertainties up to p(T) = 5 GeV/c and close to the mean value for larger p(T). The modification of the electron yield with respect to what is expected for an incoherent superposition of nucleon-nucleon collisions is evaluated by measuring the nuclear modification factor R-AA. The measurement of the R-AA in different centrality classes allows in-medium energy loss of charm and beauty quarks to be investigated. The R-AA shows a suppression with respect to unity at intermediate p(T), which increases while moving towards more central collisions. Moreover, the measured R-AA is sensitive to the modification of the parton distribution functions (PDF) in nuclei, like nuclear shadowing, which causes a suppression of the heavy--quark production at low p(T) in heavy-ion collisions at LHC.

PHYSICS LETTERS B 804, 135377, 2020. DOI: 10.1016/j.physletb.2020.135377

[P185-2020] "Measurement of the (anti-)He-3 elliptic flow in Pb-Pb collisions at root s(NN)=5.02TeV"

Acharya, S.; Adamova, D.; Adhya, S. P.; **Albuquerque, D. S. D.*; Chinellato, D. D.*; De Souza, R. D.*; Takahashi, J.***; et. al.; ALICE Collaboration

The elliptic flow (v(2)) of (anti-)He-3 is measured in Pb-Pb collisions at root s(NN)= 5.02TeV in the transverse-momentum (p(T)) range of 2-6 GeV/c for the centrality classes 0-20%, 20-40%, and 40-60% using the event-plane method. This measurement is compared to that of pions, kaons, and protons at the same center-of-mass energy. A clear mass ordering is observed at low p(T), as expected from relativistic hydrodynamics. The violation of the scaling of v(2) with the number of constituent quarks at low p(T), already observed for identified hadrons and deuterons at LHC energies, is confirmed also for (anti-)He-3. The elliptic flow of (anti-)He-3 is underestimated by the Blast-Wave model and overestimated by a simple coalescence approach based on nucleon scaling. The elliptic flow of (anti-)He-3 measured in the centrality classes 0-20% and 20-40% is well described by a more sophisticated coalescence model where the phase-space distributions of protons and neutrons are generated using the iEBE-VISHNU hybrid model with AMPT initial conditions.

PHYSICS LETTERS B 805,135414, 2020. DOI: 10.1016/j.physletb.2020.135414

[P186-2020] "Measurement of the cross section for electroweak production of a Z boson, a photon and two jets in proton-proton collisions at root s=13TeV and constraints on anomalous quartic couplings"

Sirunyan, A. M.; Tumasyan, A.; Adam, W.; **Chinellato, J. A.*; Tonelli Manganote, E. J.***; et. al.; CMS Collaboration

A measurement is presented of the cross section for electroweak production of a Z boson and a photon in association with two jets (Z gamma jj) in proton-proton collisions. The Z boson candidates are selected through their decay into a pair of electrons or muons. The process of interest, electroweak Z gamma jj production, is isolated by selecting events with a large dijet mass and a large pseudorapidity gap between the two jets. The measurement is based on data collected at the CMS experiment at root s = 13 TeV, corresponding to an integrated luminosity of 35.9 fb(-1). The observed significance of the signal is 3.9 standard deviations, where a significance of 5.2 standard deviations is expected in the standard model. These results are combined with published results by CMS at root s = 8 TeV, which leads to observed and expected respective significances of 4.7 and 5.5 standard deviations. From the 13 TeV data, a value is obtained for the signal strength of electroweak Z gamma jj production and bounds are given on quartic vector boson interactions in the framework of dimension-eight effective field theory operators.

JOURNAL OF HIGH ENERGY PHYSICS 6, 76, 2020. DOI: 10.1007/JHEP06(2020)076

[P187-2020] "Measurement of the Jet Mass Distribution and Top Quark Mass in Hadronic Decays of Boosted Top Quarks in pp Collisions at root s=13 TeV"

Sirunyan, A. M.; Tumasyan, A.; Adam, W.; **Chinellato, J. A.*; Tonelli Manganote, E. J.***; et. al.; CMS Collaboration

A measurement is reported of the jet mass distribution in hadronic decays of boosted top quarks produced in pp collisions at root s = 13 TeV. The data were collected with the CMS detector at the LHC and correspond to an integrated luminosity of 35.9 fb(-1). The measurement is performed in the lepton + jets channel of t (t) over bar events, where the lepton is an electron or muon. The products of the hadronic top quark decay t -> bW -> bq (q) over bar' are reconstructed as a single jet with transverse momentum larger than 400 GeV. The t (t) over bar cross section as a function of the jet mass is unfolded at the particle level and used to extract a value of the top quark mass of 172.6 +/- 2.5 GeV. A novel jet reconstruction technique is used for the first time at the LHC, which improves the precision by a factor of 3 relative to an earlier measurement. This highlights the potential of measurements using boosted top quarks, where the new technique will enable future precision measurements.

PHYSICAL REVIEW LETTERS 124[20], 202001, 2020. DOI: 10.1103/PhysRevLett.124.202001

[P188-2020] "Measurements with silicon photomultipliers of dose-rate effects in the radiation damage of plastic scintillator tiles in the CMS hadron endcap calorimeter"

Sirunyan, A. M.; Tumasyan, A.; Adam, W.; **Chinellato, J. A.*; Tonelli Manganote, E. J.***; et. al.; CMS Collaboration

Measurements are presented of the reduction of signal output due to radiation damage for two types of plastic scintillator tiles used in the hadron endcap (HE) calorimeter of the CMS detector. The tiles were exposed to particles produced in proton-proton (pp) collisions at the CERN LHC with a center--of-mass energy of 13 TeV, corresponding to a delivered luminosity of 50 fb(-1) . The measurements are based on readout channels of the HE that were instrumented with silicon photomultipliers, and are derived using data from several sources: a laser calibration system, a movable radioactive source, as well as hadrons and muons produced in pp collisions. Results from several irradiation campaigns using Co-60 sources are also discussed. The damage is presented as a function of dose rate. Within the range of these measurements, for a fixed dose the damage increases with decreasing dose rate.

JOURNAL OF INSTRUMENTATION 15[6], P06009, 2020. DOI: 10.1088/1748-0221/15/06/P06009

[P189-2020] "Mixed higher-order anisotropic flow and nonlinear response coefficients of charged particles in PbPb collisions at root s(NN)=2.76 and 5.02 TeV"

Sirunyan, A. M.; Tumasyan, A.; Adam, W.; **Chinellato, J. A.*; Tonelli Manganote, E. J.***; et. al.; CMS Collaboration

Anisotropies in the initial energy density distribution of the quark-gluon plasma created in high energy heavy ion collisions lead to anisotropies in the azimuthal distributions of the final-state particles known as collective anisotropic flow. Fourier harmonic decomposition is used to quantify these anisotropies. The higher-order harmonics can be induced by the same order anisotropies (linear response) or by the combined influence of several lower order anisotropies (nonlinear response) in the initial state. The mixed highe-rorder anisotropic flow and nonlinear response coefficients of charged particles are measured as functions of transverse momentum and centrality in PbPb collisions at nucleon-nucleon center-of--mass energies root s(NN) = 2.76 and 5.02 TeV with the CMS detector. The results are compared with viscous hydrodynamic calculations using several different initial conditions, aswell asmicroscopic transport model calculations. None of the models provides a simultaneous description of the mixed higher--order flow harmonics and nonlinear response coefficients.

EUROPEAN PHYSICAL JOURNAL C 80[6], 534, 2020. DOI: 10.1140/epjc/s10052-020-7834-9

[P190-2020] "Multimode exposed core fiber specklegram sensor"

Cabral, T. D.*; Fujiwara, E.; Warren-Smith, S. C.; Ebendorff--Heidepriem, H.; **Cordeiro, C. M. B.***

The inception of photonic crystal fibers (PCFs) allowed for unprecedented tailoring of waveguide properties for specialty sensing probes. Exposed core microstructured fibers (ECFs) represent a natural evolution of the PCF design for practical liquid and gas sensing. Until now, to the best of our knowledge, only single--mode or few-modes ECFs have been explored. In this Letter, we demonstrate a highly multimode ECF with a lateral access that extends throughout the whole length of the fiber. The ECF is operated as a fiber specklegram sensor for assessing properties of fluids and interrogated using a simple and low-cost setup. The probe exhibits a refractive index resolution and sensitivity of at least 4.6 x 10(-4) refractive index units (RIUs) and -10.97 RIU-1, respectively. A maximum temperature resolution up to 0.017 degrees C with a -0.20 degrees C-1 temperature sensitivity over the 23 degrees C-28 degrees C range and a liquid level sensing resolution up to 0.12 mm with -0.015 mm(-1) sensitivity over the 0.0-50.0 mm bathed the length range in water.

OPTICS LETTERS 45[12], 3212-3215, 2020. DOI: 10.1364/OL.391812

[P191-2020] "Nature inspired solid-liquid phase amphibious adhesive"

Chipara, A. C.; **Brunetto, G.***; Ozden, S.; Haspel, H.; Kumbhakar, P.; **Kukovecz, A.*; Konya, Z.***; Vajtai, R.; Chipara, M.; **Galvao, D. S.***; Tiwary, C. S.; Ajayan, P. M.

Here we report a new class of bio-inspired solid-liquid adhesive, obtained by simple mechanical dispersion of PVDF (polyvinylidene fluoride) (solid spheres) into PDMS (polydimethylsiloxane) (liquid). The adhesive behavior arises from strong solid-liquid interactions. This is a chemical reaction free adhesive (no curing time) that can be repeatedly used and is capable of instantaneously joining a large number of diverse materials (metals, ceramic, and polymer) in air and underwater. The current work is a significant advance in the development of amphibious multifunctional adhesives and presents potential applications in a range of sealing applications, including medical ones.

SOFT MATTER 16[25], 5854-5860, 2020. DOI: 10.1039/d0sm00105h

[P192-2020] "Non-linear flow modes of identified particles in Pb-Pb collisions at root S-NN=5.02 TeV"

Acharya, S.; Acosta, F. T.; Adam, J.; **Albuquerque, D. S. D.*; Chinellato, D. D.*; De Souza, R. D.*; Takahashi, J.***; et. al.; ALICE Collaboration

The p(T)-differential non-linear flow modes, v(4,22), v(5,32), v(6, 33) and v(6,222) for pi(+/-), K-+/-, K-S(0), p + (p) over bar, Lambda + (Lambda) over bar and phi-meson have been measured for the first time at root SNN = 5.02 TeV in Pb-Pb collisions with the ALICE detector at the Large Hadron Collider. The results were obtained with a multi-particle technique, correlating the identified hadrons with reference charged particles from a different pseudorapidity region. These non-linear observables probe the contribution from the second and third order initial spatial anisotropy coefficients to higher flow harmonics. All the characteristic features observed in previous p(T) -differential anisotropic flow measurements for various particle species are also present in the non-linear flow modes, i.e. increase of magnitude with increasing centrality percentile, mass ordering at low p(T)and particle type grouping in the intermediate p(T) range. Hydrodynamical calculations (iEBE--VISHNU) that use different initial conditions and values of shear and bulk viscosity to entropy density ratios are confronted with the data at low transverse momenta. These calculations exhibit a better agreement with the anisotropic flow coefficients than the non-linear flow modes. These observations indicate that non-linear flow modes can provide additional discriminatory power in the study of initial conditions as well as new stringent constraints to hydrodynamical calculations.

JOURNAL OF HIGH ENERGY PHYSICS 6, 147, 2020. DOI: 10.1007/JHEP06(2020)147

[P193-2020] "Nonequilibrium processes in repulsive binary mixtures"

Florez, P. A. S.*; Koning, M. de*

We consider rapid cooling processes in classical, three-dimensional, purely repulsive binary mixtures in which an initial infinite-temperature (ideal-gas) configuration is instantly quenched to zero temperature. It is found that such systems display two kinds of ordering processes, the type of which can be controlled by tuning the interactions between unlike particles. While strong inter-species repulsion leads to chemical ordering in terms of an unmixing process, weak repulsion gives rise to spontaneous crystallization, maintaining chemical homogeneity. This result indicates the existence of a transition in the topography of the underlying potential-energy landscape as the intra-species interaction strength is varied. Furthermore, the dual-type behavior appears to be universal for repulsive pair-interaction potential-energy functions in general, with the propensity for the crystallization process being related to their behavior in the neighborhood of zero separation.

JOURNAL OF CHEMICAL PHYSICS 152[23], 234505, 2020. DOI: 10.1063/5.0011375

[P194-2020] "Observation and confirmation of nine strong--lensing systems in Dark Energy Survey Year 1 data"

Nord, B.; Buckley-Geer, E.; Lin, H.; **Sobreira, F.***; et. al.; DES Collaboration

We describe the observation and confirmation of nine new strong gravitational lenses discovered in Year 1 data from the Dark Energy Survey (DES). We created candidate lists based on (i) galaxy group and cluster samples, and (ii) photometrically selected galaxy samples. We selected 46 candidates through visual inspection and then used the Gemini Multi-Object Spectrograph (GMOS) at the Gemini South telescope to acquire a spectroscopic follow-up of 21 of these candidates. Through an analysis of these spectroscopic follow-up data, we confirmed nine new lensing systems and rejected two candidates, and the analysis was inconclusive on 10 candidates. For each of the confirmed systems, our report measured spectroscopic properties, estimated source image-lens separations, and estimated enclosed masses as well. The sources that we targeted have an i-band surface brightness range of i(SB) similar to 22-24 mag arcsec(-2) and a spectroscopic redshift range of z(spec) similar to 0.8-2.6. The lens galaxies have a photometric redshift range of z(lens) similar to 0.3-0.7. The lensing systems range in source image-lens separation from 2 to 9 arcsec and in enclosed mass from 10(12) to 10(13) M-circle dot.

MONTHLY NOTICES OF THE ROYAL ASTRONOMICAL SOCIETY 494[1], 1308-1322, 2020. DOI: 10.1093/mnras/staa200

[P195-2020] "Optical Absorption Exhibits Pseudo-Direct Band Gap of Wurtzite Gallium Phosphide"

Silva, B. C. da*; Couto Jr., O. D. D.*; Obata, H. T.*; Lima, M. M. de; Bonani, F. D.; Oliveira, C. E. de; Sipahi, G. M.; **Iikawa, F.*; Cotta, M. A.***

Definitive evidence for the direct band gap predicted for Wurtzite Gallium Phosphide (WZ GaP) nanowires has remained elusive due to the lack of strong band-to-band luminescence in these materials. In order to circumvent this problem, we successfully obtained large volume WZ GaP structures grown by nanoparticle-crawling assisted Vapor-Liquid-Solid method. With these structures, we were able to observe bound exciton recombination at 2.14 eV with FHWM of approximately 1 meV. In addition, we have measured the optical absorption edges using photoluminescence excitation spectroscopy. Our results show a 10 K band gap at 2.19 eV and indicate a weak oscillator strength for the lowest energy band-to-band absorption edge, which is a characteristic feature of a pseudo-direct band gap semiconductor. Furthermore, the valence band splitting energies are estimated as 110 meV and 30 meV for the three highest bands. Electronic band structure calculations using the HSE06 hybrid density functional agree qualitatively with the valence band splitting energies.

SCIENTIFIC REPORTS 10[1], 7904, 2020. DOI: 10.1038/s41598-020-64809-4

[P196-2020] "Palmitic acid-coated magnetite nanocubes with high-quality crystallinity and bulk-like magnetic features"

Orozco-Henao, J. M.; **Muraca, D.***; Sanchez, F. H.; Zelis, Mendoza Zelis, P.

We have demonstrated the synthesis of high-quality monocrystalline magnetite nanocubes through the introduction of palmitic acid as surfactant in a thermal decomposition synthesis of an organic Fe precursor. Unlike the standard thermal decomposition synthesis route, we report the avoid of the reducing agent and a modification in the synthesis heating ramp. Structural and magnetic properties were investigated showing well defined cubic shaped nanoparticles with a similar to 40 nm edge and magnetic features close to bulk magnetite. We associate the bulk-like magnetic performance and properties to the highly crystalline structure of the nanocubes. In addition, we introduce a facile way to make a ligand exchange of nanocubes initial surfactant to citric acid in order to obtain biocompatible hydrophilic nanocubes. The potential application of the obtained sample in magnetic hyperthermia therapy is shown through calorimetric heating measurements on liquid dispersions of the nanocubes. We compute the Specific Absorption Rate to quantify the heating efficiency of the nanocubes.

JOURNAL OF PHYSICS D-APPLIED PHYSICS 53[38], 385001, 2020. DOI: 10.1088/1361-6463/ab9264

[P197-2020] "Probing the Effects of Strong Electromagnetic Fields with Charge-Dependent Directed Flow in Pb-Pb Collisions at the LHC"

Acharya, S.; Adamova, D.; Adler, A.; **Albuquerque, D. S. D.*; Chinellato, D. D.*; Takahashi, J.***; et. al.; A Large Ion Collider Expt Collabor

The first measurement at the LHC of charge-dependent directed flow (v(1)) relative to the spectator plane is presented for Pb-Pb collisions at root s(NN) = 5.02 TeV. Results are reported for charged hadrons and D-0 mesons for the transverse momentum intervals p(T) > 0.2 GeV/c and 3 < p(T) < 6 GeV/c in the 5%-40% and 10%-40% centrality classes, respectively. The difference between the positively and negatively charged hadron v(1) has a positive slope as a function of pseudorapidity eta, d Delta v(1)/d eta = [1.68 +/- 0.49(stat) +/- 0.41(syst)] x 10(-4). The same measurement for D-0 and (D) over bar (0) mesons yields a positive value d Delta v(1)/d eta = [4.9 +/- 1.7(stat)] +/- 0.6(syst)] x 10(-1), which is about 3 orders of magnitude larger than the one of the charged hadrons. These measurements can provide new insights into the effects of the strong electromagnetic field and the initial tilt of matter created in noncentral heavy ion collisions on the dynamics of light (u, d, and s) and heavy (c) quarks. The large difference between the observed Delta v(1) of charged hadrons and D-0 mesons may reflect different sensitivity of the charm and light quarks to the early time dynamics of a heavy ion collision. These observations challenge some recent theoretical calculations, which predicted a negative and an order of magnitude smaller value of d Delta v(1)/d eta for both light flavor and charmed hadrons.

PHYSICAL REVIEW LETTERS 125[2], 022301, 2020. DOI: 10.1103/PhysRevLett.125.022301

[P198-2020] "Probing the Site-Selective Doping in SrSnO3:Eu Oxides and Its Impact on the Crystal and Electronic Structures Using Synchrotron Radiation and DFT Simulations"

Chantelle, L.; Oliveira, A. L. M. de; Kennedy, B. J.; Maul, J.; Silva, M. R. S.; Duarte, T. M.; Albuquerque, A. R.; Sambrano, J. R.; **Landers, R.***; Siu-Li, M.; Longo, E.; Santos, I. M. G. dos

The impact of Eu3+ doping at the Sr2+ and Sn4+ sites in SrSnO3 on its structural and electronic properties was studied and correlated with the photocatalytic efficiency. The compounds were synthesized using a modified Pechini method. Refinement of the synchrotron X-ray diffraction (S-XRD) data showed that the samples had an orthorhombic Pbnm symmetry. The incorporation of Eu into the lattice led to increased short- and long--range disorder, inducing additional distortion in the SnO6. XANES measurements revealed that mixed Eu valences (Eu3+ and Eu2+) were present in Eu-doped samples, and DFT calculations confirmed the presence of these ions at Sr2+/Sr4+ sites in the SrSnO3, resulting in changes in the electronic behavior. The catalytic performance toward Remazol yellow dye photodegradation and the catalysts' surface properties were also evaluated. The catalytic efficiency followed the order of Sr(Sn0.99Eu0.01) SnO3 > (Sr0.99Eu0.01)SnO3 > SrSnO3. The order was clearly related to selected-site doping that changed the degree of the inter- and intraoctahedral distortion and the introduction of different Eu midgap states, which apparently favor charge separation upon photoexcitation during photocatalysis. The results shown here are of great importance to the functionalization of SrSnO3 and other perovskite materials by lanthanoid ions, especially Eu3+, for effective applications as photocatalysts.

INORGANIC CHEMISTRY 59 [11], 7666-7680, 2020. DOI: 10.1021/acs.inorgchem.0c00664

[P199-2020] "PyScratch: An ease of use tool for analysis of scratch assays"

Garcia-Fossa, F.; **Gaal, V.***; Jesus, M. B.

Background and objective: Image acquisition has greatly benefited from the automation of microscopes and has been followed by an increasing amount and complexity of data acquired. Here, we present the PyScratch, a new tool for processing spatial and temporal information from scratch assays. PyScratch is an open-source software implemented in Python that analyses the migration area in an automated fashion. Methods: The software was developed in Python. Wound healing assays were used to validate its performance. The images were acquired using Cytation 5 (TM) during 60 h. Data were analyzed using One-Way ANOVA. Results: PyScratch performed a robust analysis of confluent cells, showing that high plating density affects cell migration. Additionally, PyScratch was approximately six times faster than a semi-automated analysis. Conclusions: PyScratch offers a user-friendly interface allowing researches with little or no programming skills to perform quantitative analysis of in vitro scratch assays.

COMPUTER METHODS AND PROGRAMS IN BIOMEDICINE 193, 105476, 2020. DOI: 10.1016/j.cmpb.2020.105476

[P200-2020] "Raman spectra of multilayer graphene under high temperatures"

Alaferdov, A. V.*; Savu, R.; Fantini, C.; Cancado, L. G.; Moshkalev, S. A.

For graphitic materials, Raman technique is a common method for temperature measurements through analysis of phonon frequencies. Temperature (T) induced downshift of the bond-stretching G mode (Delta G) is well known, but experimentally obtained thermal coefficients Delta G/Delta Tvary considerably between diverse works. Further, Delta G/Delta T coefficients usually were evaluated for relatively low temperatures and found to differ strongly for mono, a few and multilayer graphene. We studied G band behavior in freely suspended multilayer graphene flakes (or graphite nanoflakes) under localized heating by a laser beam. Analysis of Stokes and anti-Stokes signals showed that G band has a complex structure and can be deconvoluted into several peaks that demonstrate distinctly different behavior under heating. A plausible assumption is that these peaks correspond to several groups of graphitic layers (surface, near-surface and bulk) and then different thermal coefficients were determined for these groups. This behavior can be explained by decreasing interaction between surface layers and underlying material at high temperatures that affects especially vibrational properties of a few outermost layers. Estimates of temperatures using anti-Stokes/Stokes intensity ratio (I-aS/I-S) were also done to give results comparable with those obtained from G band downshift,T-Delta G approximate to T-aS/S, supporting the proposed model. The range of temperatures obtained by laser heating, as evaluated by both methods, was from 450 to 1200 K.

JOURNAL OF PHYSICS-CONDENSED MATTER 32[38], 385704, 2020. DOI: 10.1088/1361-648X/ab95ce

[P201-2020] "Real-Time Non-invasive Assessment of Cerebral Hemodynamics With Diffuse Optical Spectroscopies in a Neuro Intensive Care Unit: An Observational Case Study"

Forti, R. M.*; Katsurayama, M.; Menko, J.; Valler, L.; **Quiroga, A.*;** Falcao, A. L. E.; Li, Li M.; **Mesquita, R. C.***

Prevention of secondary damage is an important goal in the treatment of severe neurological conditions, such as major head trauma or stroke. However, there is currently a lack of non-invasive methods for monitoring cerebral physiology. Diffuse optical methods have been proposed as an inexpensive, non-invasive bedside monitor capable of providing neurophysiology information in neurocritical patients. However, the reliability of the technique to provide accurate longitudinal measurement during the clinical evolution of a patient remains largely unaddressed. Here, we report on the translation of a hybrid diffuse optical system combining frequency domain diffuse optical spectroscopy (FD-DOS) and diffuse correlation spectroscopy (DCS) for real-time monitoring of cerebral physiology in a neuro intensive care unit (neuro-ICU). More specifically, we present a case study of a patient admitted with a high-grade aneurysmal subarachnoid hemorrhage, who was monitored throughout hospitalization. We show that the neurophysiological parameters measured by diffuse optics at the bedside are consistent with the clinical evolution of the patient at all the different stages following its brain lesion. These data provide support for clinical translation of DOS/DCS as a useful biomarker of neurophysiology in the neuro-ICU, particularly in locations where other clinical resources are limited.

FRONTIERS IN MEDICINE 7[147], 2020. DOI: 10.3389/fmed.2020.00147

[P202-2020] "Sarin and Air Permeation Through a Nanoporous Graphene"

Maria, M. A.*; Fonseca, A. F.*

Sarin gas is a dangerous chemical warfare agent (CWA). It is a nerve agent capable of bringing a person to death in about 15 minutes. A lethal concentration of sarin molecules in air is about 30 mg/m(3). Experimental research on this gas requires very careful safety protocols for handling and storage. Therefore, theoretical and computational studies on sarin gas are very welcome and might provide important safe guides towards the management of this lethal substance.

In this work, we investigated the interactions between sarin, air and nanoporous graphene, using tools of classical molecular dynamics simulations. Aiming to cast some light in the possible sarin selective filtration by graphene, we designed a bipartite simulation box with a porous graphene nanosheet placed at the middle. Sarin and air molecules were initially placed only on one side of the box so as to create an initial pressure towards the passage of both to the other side. The box dimensions were chosen so that the hole in the graphene was the only possible way through which sarin and air molecules can get to the other side of the box. The number of molecules that passed through the hole in graphene was monitored during 10 ns of simulation and the results for different temperatures were compared. The results show that, as far as the size of the holes are small, van der Waals forces between graphene and the molecules play a significant role on keeping sarin near graphene, at room temperature.

MRS ADVANCES 5[27-28][SI], 1475-1482, 2020. DOI: 10.1557/adv.2020.149

[P203-2020] "Search for an excited lepton that decays via a contact interaction to a lepton and two jets in proton--proton collisions at root s=13 TeV"

Sirunyan, A. M.; Tumasyan, A.; Adam, W.; **Chinellato, J. A.*; Tonelli Manganote, E. J.***; et. al.; CMS Collaboration

Results are presented from a search for events containing an excited lepton (electron or muon) produced in association with an ordinary lepton of the same flavor and decaying to a lepton and two hadronic jets. Both the production and the decay of the excited leptons are assumed to occur via a contact interaction with a characteristic energy scale ?. The branching fraction for the decay mode under study increases with the mass of the excited lepton and is the most sensitive channel for very heavy excited leptons. The analysis uses a sample of proton-proton collisions collected by the CMS experiment at the LHC at root s = 13 TeV, corresponding to an integrated luminosity of 77.4 fb(-1). The four-body invariant mass of the two lepton plus two jet system is used as the primary discriminating variable. No significant excess of events beyond the expectation for standard model processes is observed. Assuming that ? is equal to the mass of the excited leptons, excited electrons and muons with masses below 5.6 and 5.7 TeV, respectively, are excluded at 95% confidence level. These are the best limits to date.

JOURNAL OF HIGH ENERGY PHYSICS 5, 052, 2020. DOI: 10.1007/JHEP05(2020)052

[P204-2020] "Search for dijet resonances using events with three jets in proton-proton collisions at root s=13 TeV"

Sirunyan, A. M.; Tumasyan, A.; Adam, W.; **Chinellato, J. A.*; Tonelli Manganote, E. J.*;** et. al.; CMS Collaboration

A search for a narrow resonance with a mass between 350 and 700 GeV, and decaying into a pair of jets, is performed using proton-proton collision events containing at least three jets. The data sample corresponds to an integrated luminosity of 18.3 fb(-1) recorded at root s = 13 TeV with the CMS detector. Data are collected with a technique known as "data scouting", in which the events are reconstructed, selected, and recorded at a high rate in a compact form by the high--level trigger. The three-jet final state provides sensitivity to lower resonance masses than in previous searches using the data scouting technique. The spectrum of the dijet invariant mass, calculated from the two jets with the largest transverse momenta in the event, is used to search for a resonance. No significant excess over a smoothly falling background is found. Limits at 95% confidence level are set on the production cross section of a narrow dijet resonance and compared with the cross section of a vector dark matter mediator coupling to dark matter particles and quarks. Translating to a model where the narrow resonance interacts only with quarks, upper limits on this coupling range between 0.10 and 0.15, depending on the resonance mass. These results represent the most stringent upper limits in the mass range between 350 and 450 GeV obtained with a flavor-inclusive dijet resonance search.

PHYSICS LETTERS B 805, 135448, 2020. DOI: 10.1016/j.physletb.2020.135448

[P205-2020] "Search for direct top squark pair production in events with one lepton, jets, and missing transverse momentum at 13 TeV with the CMS experiment"

Sirunyan, A. M.; Tumasyan, A.; Adam, W.; **Chinellato, J. A.*; Tonelli Manganote, E. J.*;** et. al.; CMS Collaboration

A search for direct top squark pair production is presented. The search is based on proton-proton collision data at a center--of-mass energy of 13 TeV recorded by the CMS experiment at the LHC during 2016, 2017, and 2018, corresponding to an integrated luminosity of 137 fb(-1). The search is carried out using events with a single isolated electron or muon, multiple jets, and large transverse momentum imbalance. The observed data are consistent with the expectations from standard model processes. Exclusions are set in the context of simplified top squark pair production models. Depending on the model, exclusion limits at 95% confidence level for top squark masses up to 1.2 TeV are set for a massless lightest supersymmetric particle, assumed to be the neutralino. For models with top squark masses of 1 TeV, neutralino masses up to 600 GeV are excluded.

JOURNAL OF HIGH ENERGY PHYSICS 5, 032, 2020. DOI: 10.1007/JHEP05(2020)032

[P206-2020] "Single-phase and binary phase nanogranular ferrites for magnetic hyperthermia application"

Thandapani, P.*; Viswanathan, M. R.; Araujo, M. V.; Bakuzis, A. F.; **Beron, F.*;** Thirumurugan, A.; Denardin, J. C.; Jimenez, J. A.; Fakhrabadi, A. A.

The study demonstrates the performance of heating efficiency in single-phase and binary phase spinel ferrite nanosystems. Ferrimagnetic cobalt ferrite (CoFe2O4) (CFO) and superparamagnetic copper ferrite/copper oxide (CuFe2O4/CuO) (CuF) nanosystems of different particle sizes were synthesized through a microwave-assisted coprecipitation method. The heating behavior was observed in range of both field amplitudes (8-24 kA/m at 516 kHz) and frequencies (325-973 kHz at 12 kA/m). The heating efficiency was analyzed and compared by means of particle size, magnetization, effective anisotropy constant, and Neel relaxation mechanism. Indeed, the heating rate was maximized in larger ferrite particles with low effective anisotropy constant. Moreover, though the magnetization and effective anisotropy constant of single-phase CoFe2O4 nanoparticles were higher, the binary phase CuFe2O4/CuO nanosystems of similar crystallite size (28 nm) exhibited superior heating efficiency (4.21 degrees C/s). For a field amplitude and frequency of 24 kA/m and 516 kHz, the heating rate of CuF and CFO ferrites with different crystallite sizes decreased in the order of 4.21 > 2.14 > 0.58 > 0.52 degrees C/s for 29 nm > 25 nm > 12 nm > 15 nm, respectively. The results emphasize that binary phase ferrite nanoparticles are better thermoseeds than the single--phase ferrites for the magnetic hyperthermia application.

JOURNAL OF THE AMERICAN CERAMIC SOCIETY 103[9], 5086-5097, 2020. DOI: 10.1111/jace.17175

[P207-2020] "Spectral variability of a sample of extreme variability quasars and implications for the MgII broad-line region"

Yang, Q.; Shen, Y.; Chen, Y. C.; **Sobreira, F.*;** et. al.;

We present new Gemini/GMOS optical spectroscopy of 16 extreme variability quasars (EVQs) that dimmed bymore than 1.5mag in the g band between the Sloan Digital Sky Survey (SDSS) and the Dark Energy Survey epochs (separated by a few years in the quasar rest frame). These EVQs are selected from quasars in the SDSS Stripe 82 region, covering a redshift range of 0.5 < z < 2.1. Nearly half of these EVQs brightened significantly (by more than 0.5 mag in the g band) in a few years after reaching their previous faintest state, and some EVQs showed rapid (non-blazar) variations of greater than 1-2 mag on time--scales of only months. To increase sample statistics, we use a supplemental sample of 33 EVQs with multi-epoch spectra from SDSS that cover the broad Mg II lambda 2798 line. Leveraging on the large dynamic range in continuum variability between the multi-epoch spectra, we explore the associated variations in the broad MgII line, whose variability properties have not been well studied before. The broad MgII flux varies in the same direction as the continuum flux, albeit with a smaller amplitude, which indicates at least some portion of Mg II is reverberating to continuum changes. However, the full width at half-maximum (FWHM) of Mg II does not vary accordingly as continuum changes for most objects in the sample, in contrast to the case of the broad Balmer lines. Using the width of broad MgII to estimate the black hole mass with single epoch spectra therefore introduces a luminosity-dependent bias.

MONTHLY NOTICES OF THE ROYAL ASTRONOMICAL SOCIETY 493[4], 5773-5787, 2020. DOI: 10.1093/mnras/staa645

[P208-2020] "Stellar mass as a galaxy cluster mass proxy: application to the Dark Energy Survey redMaPPer clusters"

Palmese, A.; Annis, J.; Burgad, J.; **Sobreira, F.*;** et. al.; DES Collaboration

We introduce a galaxy cluster mass observable, mu(*), based on the stellar masses of cluster members, and we present results for the Dark Energy Survey (DES) Year 1 (Y1) observations. Stellar masses are computed using a Bayesian model averaging method, and are validated for DES data using simulations and COSMOS data. We show that mu(*) works as a promising mass proxy by comparing our predictions to X-ray measurements. We measure the X-ray temperature-mu(*) relation for a total of 129 clusters matched between the wide-field DES Y1 redMaPPer catalogue and Chandra and XMM archival observations, spanning the redshift range 0.1 < z < 0.7. For a scaling relation that is linear in logarithmic space, we find a slope of alpha = 0.488 +/- 0.043 and a scatter in the X-ray temperature at fixed mu(*) of sigma(lnTX)vertical bar mu(*) = 0.266(-0.020)(+0.019) for the joint sample. By using the halo mass scaling relations of the X-ray temperature from the Weighing the Giants program, we further derive the mu(star)- conditioned scatter inmass, finding sigma(lnM)vertical bar mu(*) = 0.26(-0.10)(+0.15). These results are competitive with well--established cluster mass proxies used for cosmological analyses, showing that mu(*) can be used as a reliable and physically motivated mass proxy to derive cosmological constraints.

MONTHLY NOTICES OF THE ROYAL ASTRONOMICAL SOCIETY 493[4], 4591-4606, 2020. DOI: 10.1093/mnras/staa526

[P209-2020] "Strange hadron production in pp and pPb collisions at root(NN)-N-s=5.02 TeV"

Sirunyan, A. M.; Tumasyan, A.; Adam, W.; **Chinellato, J. A.*; Tonelli Manganote, E. J.***; et. al.; CMS Collaboration

The transverse momentum (pT) distributions of Lambda, Xi(-), and Omega(-) baryons, their antiparticles, and K-S(0) mesons are measured in proton-proton (pp) and proton-lead (pPb) collisions at a nucleon-nucleon center-of-mass energy of 5.02 TeV over a broad rapidity range. The data, corresponding to integrated luminosities of 40.2 nb(-1) and 15.6 mu b(-1) for pp and pPb collisions, respectively, were collected by the CMS experiment. The nuclear modification factor R-pPb, which is defined as the ratio of the particle yield in pPb collisions and a scaled pp reference, is measured for each particle. A strong dependence on particle species is observed in the pT range from 2 to 7 GeV, where R-pPb for K-S(0) is consistent with unity, while an enhancement ordered by strangeness content and/or particle mass is observed for the three baryons. In pPb collisions, the strange hadron production is asymmetric about the nucleon--nucleon center-of-mass rapidity. Enhancements, which depend on the particle type, are observed in the direction of the Pb beam. The results are compared with predictions from EPOS LHC, which includes parametrized radial flow. The model is in qualitative agreement with the R-pPb data, but fails to describe the dependence on particle species in the yield asymmetries measured away from midrapidity in pPb collisions.

PHYSICAL REVIEW C 101[6], 064906, 2020. DOI: 10.1103/PhysRevC.101.064906

[P210-2020] "Supramolecular architecture and electrical conductivity in organic semiconducting thin films"

Fernandes, J. D.; Maximino, M. D.; **Braunger, M. L.***; Pereira, M. S.; Olivati, C. de A.; Constantino, C. J. L.; Alessio, P.

Organic thin films are an essential component of the structure of optical and electronic devices. However, the optical and electrical properties of these films depend on their supramolecular architecture, which may vary according to the techniques used to manufacture them. Here, the correlation between conductivity and supramolecular architecture was investigated. The supramolecular architecture was analyzed in terms of the molecular organization and J- or H-aggregation established during the fabrication of perylene tetracarboxylic diimide (PTCD) nanometric films. Three deposition techniques, Langmuir-Schaefer (LS), Langmuir-Blodgett (LB), and Physical Vapor Deposition (PVD), were evaluated. The UV-vis absorption spectra indicated that LS, LB, and PVD films grow homogeneously. Also, the presence of J and H aggregates was observed for all films, the H aggregates prevailing for the LB film. The FTIR measurements suggested that the molecular organization is similar for LS and LB films, with a tendency to form head--on organization onto a solid substrate. For the PVD film, the perylene macrocycles are inclined approximately 45 degrees relative to the substrate. AFM measurements indicated a homogenous surface for all films. In terms of electrical conductivity, the highest conductivity was found for LS, followed by LB and PVD. The conductivity values were interpreted in terms of molecular organization and J- or H-aggregate formation.

PHYSICAL CHEMISTRY CHEMICAL PHYSICS 22[24], 13554-13562, 2020. DOI: 10.1039/d0cp01293a

[P211-2020] "Supramolecular Ordering and Reactions of a Chlorophenyl Porphyrin on Ag(111)"

Ferreira, R. C. de C.*; Paz, A. P.; Mowbray, D. J.; **Roulet, J. Y.*; Landers, R.*; Siervo, A. de***

Surface-assisted Ullmann-type coupling reactions are a potential bottom-up approach for building tailored low--dimensional materials with novel physical and chemical properties. In this investigation combining scanning tunneling microscopy (STM), density functional theory (DFT), and X-ray photoelectron spectroscopy (XPS),

we study the adsorption behavior, supramolecular ordering, and chemical and physical changes upon annealing of a 5,10,15,20-tetrakis(4-chlorophenyl) porphyrin (Cl4TPP) on the Ag(111) surface. At room temperature, well-ordered two-dimensional (2D) assemblies grow preferentially along the < 1 (1) over bar0 > directions, revealing the coexistence of two distinguishable porous and zigzag structures and lattice parameters. Our DFT calculations show that Cl4TPP adsorbs in the typical saddle-shape conformation on Ag(111) and that the coexistence of these two overlayers is due to translations between nearly isoenergetic adsorption sites. Furthermore, to self-polymerize the organic mesh via an on-surface Ullmann-type coupling reaction, we performed an STM and XPS study of the system upon annealing, following the chemical and structural modifications above room temperature. Under these conditions, we obtain a highly compact 2D framework composed of dechlorinated molecules.

JOURNAL OF PHYSICAL CHEMISTRY C 124[26], 14220-14228, 2020. DOI: 10.1021/acs.jpcc.0c02953

[P212-2020] "Synchronization and spatial patterns in forced swarmalators"

Lizarraga, J. U. F.; **Aguiar, M. A. M. de***

Swarmalators are particles that exhibit coordinated motion and, at the same time, synchronize their intrinsic behavior, represented by internal phases. Here, we study the effects produced by an external periodic stimulus over a system of swarmalators that move in two dimensions. The system represents, for example, a swarm of fireflies in the presence of an external light source that flashes at a fixed frequency. If the spatial movement is ignored, the dynamics of the internal variables are equivalent to those of Kuramoto oscillators. In this case, the phases tend to synchronize and lock to the external stimulus if its intensity is sufficiently large. Here, we show that in a system of swarmalators, the force also shifts the phases and angular velocities leading to synchronization with the external frequency. However, the correlation between phase and spatial location decreases with the intensity of the force, going to zero at a critical intensity that depends on the model parameters. In the regime of zero correlation, the particles form a static symmetric circular distribution, following a simple model of aggregation. Interestingly, for intermediate values of the force intensity, different patterns emerge, with the particles spiraling or splitting in two clusters centered at opposite sides of the stimulus' location. The spiral and two-cluster patterns are stable and active. The two clusters slowly rotate around the source while exchanging particles, or separate and collide repeatedly, depending on the parameters.

CHAOS 30[5], 053112, 2020. DOI: 10.1063/1.5141343

[P213-2020] "Synthesis of highly stable Fe/FeOx@citrate colloids with strong magnetic response by mechanochemistry and coprecipitation for biomedical and environmental applications"

Medina, G. A. M.; Fernandez van Raap, M. B.; Coral, D. F.; **Muraca, D.*;** Sanchez, F. H.

We present a simple, scalable, and low-cost route for producing aqueous colloids of nanometer size Fe cores coated with iron oxide and stabilized with sodium citrate. The Fe cores were obtained by mechanosynthesis by means of a highly exothermic solid-state reaction between FeCl3 and Mg, in a dispersive inert NaCl medium. The optimal experimental conditions for achieving a full reaction were determined with a Retsch 2000 oscillatory mill. Then the production yield was successfully 16-fold scaled using a rotatory Fritsch Pulverissete 7 mill. To provide biocompatibility and facilitate colloid stabilization, the Fe cores were coated with a Fe-oxide shell produced by chemical coprecipitation, and finally, the system Fe/FeOx was functionalized with sodium citrate in water. The so-obtained Fe/FeOx@Cit (4/3 < x < 3/2) nanoparticles have a mean size of about 11-12 nm, specific saturation magnetization around 130 Am-2/kg(Fe) and zeta-potential of -40 mV. The time dependence of the reaction progress yyycould be described by a simple function of the mass ratio of milling balls to processed material and time. The resultant colloids are excellent candidates for biomedical and environmental remediation applications.

JOURNAL OF MAGNETISM AND MAGNETIC MATERIALS 508 , 166759, 2020. DOI: 10.1016/j.jmmm.2020.166759

[P214-2020] "Terahertz optical fibers [Invited]"

Islam, M. S.; **Cordeiro, C. M. B.***; Franco, M. A. R.; Sultana, J.; Cruz, A. L. S.; Abbott, D.

Lying between optical and microwave ranges, the terahertz band in the electromagnetic spectrum is attracting increased attention. Optical fibers are essential for developing the full potential of complex terahertz systems. In this manuscript, we review the optimal materials, the guiding mechanisms, the fabrication methodologies, the characterization methods and the applications of such terahertz waveguides. We examine various optical fiber types including tube fibers, solid core fiber, hollow-core photonic bandgap, anti-resonant fibers, porous--core fibers, metamaterial-based fibers, and their guiding mechanisms. The optimal materials for terahertz applications are discussed. The past and present trends of fabrication methods, including drilling, stacking, extrusion and 3D printing, are elaborated. Fiber characterization methods including different optics for terahertz time-domain spectroscopy (THz-TDS) setups are reviewed and application areas including short-distance data transmission, imaging, sensing, and spectroscopy are discussed.

OPTICS EXPRESS 28[11], 16089-16117, 2020. DOI: 10.1364/OE.389999

[P215-2020] "The indirect paths to cascading effects of extinctions in mutualistic networks"

Pires, M. M.; O'Donnell, J. L.; Burkle, L. A.; Diaz-Castelazo, C.; Hembry, D. H.; Yeakel, J. D.; Newman, E. A.; Medeiros, L. P.; **Aguiar, M. A. M. de***; Guimaraes Jr., P. R.

Biodiversity loss is a hallmark of our times, but predicting its consequences is challenging. Ecological interactions form complex networks with multiple direct and indirect paths through which the impacts of an extinction may propagate. Here we show that accounting for these multiple paths connecting species is necessary to predict how extinctions affect the integrity of ecological networks. Using an approach initially developed for the study of information flow, we estimate indirect effects in plant-pollinator networks and find that even those species with several direct interactions may have much of their influence over others through long indirect paths. Next, we perform extinction simulations in those networks and show that although traditional connectivity metrics fail in the prediction of coextinction patterns, accounting for indirect interaction paths allows predicting species' vulnerability to the cascading effects of an extinction event. Embracing the structural complexity of ecological systems contributes towards a more predictive ecology, which is of paramount importance amid the current biodiversity crisis.

ECOLOGY 101[7], e03080, 2020. DOI: 10.1002/ecy.3080

[P216-2020] "The Liquid Argon In A Testbeam (LArIAT) experiment"

Acciarri, R.; Adams, C.; Asaadi, J. A.; **Dedin, P.*; Gratieri, D. R.*; Kemp, E.*; Machado, A. A. B.*; Mendes Santos, L.*; Passarelli Gelli, B.*; Reggiani Guzzo, M.*; Soares Nunes, M.*; Segreto, E.***; et. al.; LArIAT Collaboration

The LArIAT liquid argon time projection chamber, placed in a tertiary beam of charged particles at the Fermilab Test Beam Facility, has collected large samples of pions, muons, electrons, protons, and kaons in the momentum range similar to 300-1400 MeV/c. This paper describes the main aspects of the detector and beamline, and also reports on calibrations performed for the detector and beamline components.

JOURNAL OF INSTRUMENTATION 15[4], P04026, 2020. DOI: 10.1088/1748-0221/15/04/P04026

[P217-2020] "The role of vibrational temperature variations in a pulsed dielectric barrier discharge plasma device"

Nascimento, F. do; Moshkalev, S.; **Machida, M.***

The use of dielectric barrier discharge (DBD) plasmas has become a practical way to carry out surface treatment where precise control of the plasma parameters, such as rotational and vibrational temperatures (T-rot and T-vib), is required. As the T-vib of an atmospheric pressure plasma jet appears to be the most important parameter related to the improvement of surface treatments, in this work, we analysed two methods to increase the values of T-vib in a DBD plasma jet device. One of the methods is to reduce the exit size (o) of the DBD reactor, which results in an increase in the measured T-vib values, due to an increase in the pressure inside the reactor. The other method is to change the gas flow rate (GFR) used to produce the plasma jets. This leads to a T-vib reduction when the GFR is increased in the case of using helium or nitrogen as the working gas, but the opposite happens (an increase in the T-vib values) when argon is used, with different phenomena causing the variation of T-vib in each situation.

CONTRIBUTIONS TO PLASMA PHYSICS, 2020. DOI: 10.1002/ctpp.201900046

[P218-2020] "Thermodynamic signatures of an antiferromagnetic quantum critical point inside a superconducting dome"

Carvalho, V. S. de*; Chubukov, A. V.; Fernandes, R. M.

Recent experiments in unconventional superconductors, and in particular iron-based materials, have reported evidence of an antiferromagnetic quantum critical point (AFM-QCP) emerging inside the superconducting dome of the phase diagram. Fluctuations associated with such an AFM-QCP are expected to promote unusual temperature dependencies of thermodynamic quantities. Here, we compute the T dependence of the specific heat C(T) deep inside a fully gapped s(+ -) superconducting state as the AFM-QCP is approached. We find that at the AFM-QCP, the specific heat C(T) vanishes quadratically with temperature, as opposed to the typical exponential suppression seen in fully gapped BCS superconductors. This robust result is due to a nonanalytic contribution to the free energy arising from the general form of the bosonic (AFM) propagator in the SC state. Away from the AFM-QCP, as temperature is lowered, C(T) shows a crossover from a T-2 behavior to an exponential behavior, with the crossover temperature scale set by the value of the superconducting gap and the distance to the QCP. We argue that these features in the specific heat can be used to unambiguously determine the existence of AFM-QCPs inside the superconducting domes of iron-based and other fully gapped unconventional superconductors.

PHYSICAL REVIEW B 102[4], 045125, 2020. DOI: 10.1103/PhysRevB.102.045125

[P219-2020] "Three-dimensional carbon nanotube networks from beta zeolite templates: Thermal stability and mechanical properties"

Oliveira, E. F.*; Machado, L. D.; Baughman, R. H.; **Galvao, D. S.***

Zeolite-templated carbons (ZTC) are structures synthesized via chemical vapor deposition of precursors inside sacrificial zeolites, with diverse applications. In spite of the interest in ZTC, little is known regarding their mechanical properties. Here, we investigate the thermal and mechanical behaviors of three-dimensional beta zeolite-templated carbon nanotube networks (BZCN). These networks are topologically generated by inserting carbon nanotubes (CNTs) into zeolite channels and connecting them using X-type junctions. We considered two cases, one with the tubes filling all zeolite channels (HD-BZCN) and the other with just partial filling (LD-BZCN). Fully atomistic reactive molecular dynamics (MD) simulations show that the networks exhibit high thermal stability (up to 1000 K). When compressed, the structures can withstand very large strains without fracturing (> 50% for HD-BZCN and > 70% for LD-BZCN). LD-BZCN can be stretched over 100% without fracturing.

COMPUTATIONAL MATERIALS SCIENCE 182, 109781, 2020. DOI: 10.1016/j.commatsci.2020.109781

[P220-2020] "Time evolution of the behaviour of Brazilian legislative Representatives using a complex network approach"

Marenco, L.; Carmona, H. A.; Cardoso, F. M.; Andrade Jr., J. S.; **Cesar, C. L.***

The follow up of Representative behavior after elections is imperative for a democratic Representative system, at the very least to punish betrayal with no re-election. Our goal was to show how to follow Representatives' and how to show behavior in real situations and observe trends in political crises including the onset of game changing political instabilities. We used correlation and correlation distance matrices of Brazilian Representative votes during four presidential terms. Re-ordering these matrices with Minimal Spanning Trees displays the dynamical formation of clusters for the sixteen year period, which includes one Presidential impeachment. The reordered matrices, colored by correlation strength and by the parties clearly show the origin of observed clusters and their evolution over time. When large clusters provide government support cluster breaks, political instability arises, which could lead to an impeachment, a trend we observed three years before the Brazilian President was impeached. We believe this method could be applied to foresee other political storms.

PLOS ONE 15[2], e0226504, 2020. DOI: 10.1371/journal.pone.0226504

[P221-2020] "TiO2/Nb2O5/carbon xerogel ternary photocatalyst for efficient degradation of 4-chlorophenol under solar light irradiation"

Moraes, N. P.; Torezin, F. A.; Dantas, G. V. J.; Sousa, J. G. M. de; Valim, R. B.; Rocha, R. da S.; **Landers, R.*;** Silva, M. L. G. P. da; Rodrigues, L. A.

This study examines the development of ternary photocatalysts based on titanium dioxide, niobium oxide, and carbon xerogel, aimed at increasing photocatalytic efficiency under solar light irradiation.

The modifications proposed are focused on diminishing charge recombination and enhancing visible light sensitivity. The new photocatalyst was prepared using discarded titanium and niobium scraps and chips, whilst black wattle tannin was used as the carbon source. The X-ray diffractometry results show that the anatase form of titanium dioxide is present in the samples, whereas the niobium oxide presents itself in the amorphous structure. The incorporation of both carbon xerogel and niobium oxide into the TiO2 is confirmed by the infrared and energy dispersive spectroscopies. The diffuse reflectance results show that the materials containing carbon xerogel present a significantly higher visible light absorption, whilst the combined effect of the modifications proposed caused the gap energy of the ternary material to drop noticeably. The photocatalytic efficiency of the ternary material was superior to the ones found for the pure oxides and binary material, probably due to its lower value of bandgap and enhanced charge separation efficiency, as confirmed by the electrochemical impedance tests.

CERAMICS INTERNATIONAL 46[10], A,14505-14515, 2020. DOI: 10.1016/j.ceramint.2020.02.249

[P222-2020] "Tunneling-current-induced local excitonic luminescence in p-doped WSe(2)monolayers"

Roman, R. J, P.*; Auad, Y.*; Grasso, L.*; Alvarez, F.*; Barcelos, I. D.; **Zagonel, L. F.***

We have studied the excitonic properties of exfoliated tungsten diselenide (WSe2) monolayers transferred to gold substrates using the tunneling current in a Scanning Tunneling Microscope (STM) operated in air to excite the light emission locally. In obtained spectra, emission energies are independent of the applied bias voltage and resemble photoluminescence (PL) results, indicating that, in both cases, the light emission is due to neutral and charged exciton recombination. Interestingly, the electron injection rate, that is, the tunneling current, can be used to control the ratio of charged to neutral exciton emission. The obtained quantum yield in the transition metal dichalcogenide (TMD) is similar to 5 x 10(-7)photons per electron. The proposed excitation mechanism is the direct injection of carriers into the conduction band. The monolayer WSe(2)presents bright and dark defects spotted by STM images performed under UHV. STS confirms the sample as p-doped, possibly as a net result of the observed defects. The presence of an interfacial water layer decouples the monolayer from the gold support and allows excitonic emission from the WSe(2) monolayer. The creation of a water layer is an inherent feature of the sample transferring process due to the ubiquitous air moisture. Consequently, vacuum thermal annealing, which removes the water layer, quenches excitonic luminescence from the TMD. The tunneling current can locally displace water molecules leading to excitonic emission quenching and to plasmonic emission due to the gold substrate. The present findings extend the use and the understanding of STM induced light emission (STM-LE) on semiconducting TMDs to probe exciton emission and dynamics with high spatial resolution.

NANOSCALE 12[25], 13460-13470, 2020. DOI: 10.1039/d0nr03400b

[P223-2020] "Two-dimensional disordered Mott metal-insulator transition"

Suarez-Villagran, M. Y.; Mitsakos, N.; Lee, T. H.; Dobrosavljevic, V; Miller Jr., J. H.; **Miranda, E.***

We studied several aspects of the Mott metal-insulator transition in the disordered case. The model on which we based our analysis is the disordered Hubbard model, which is the simplest model capable of capturing the Mott metal-insulator transition. We investigated this model through statistical dynamical mean-field theory (statDMFT). This theory is a natural extension of dynamical mean-field theory (DMFT), which has been used with relative success in the past several years with the purpose of describing the Mott transition in the clean case. As is the case for the latter theory, statDMFT incorporates the electronic correlation effects only in their local manifestations. Disorder, on the other hand, is treated in such a way as to incorporate Anderson localization effects. With this technique, we analyzed the disordered two--dimensional Mott transition, using the quantum Monte Carlo algorithm to solve the associated single-impurity problems. We found spinodal lines at which the metal and insulator ceased to be metastable. We also studied spatial fluctuations of local quantities, such as self-energy and local Green's function, and showed the appearance of metallic regions within the insulator and vice versa. We carried out an analysis of finite-size effects and showed that, in agreement with the theorems of Imry and Ma [Y. Imry and S. K. Ma, Phys. Rev. Lett. 35, 1399 (1975).], the first-order transition is smeared in the thermodynamic limit. We analyzed transport properties by means of a mapping to a random classical resistor network and calculated both the average current and its distribution across the metal-insulator transition.

PHYSICAL REVIEW B 101[23], 235112, 2020. DOI: 10.1103/PhysRevB.101.235112

[P224-2020] "Two-Photon Emissive Dyes Based on Push-Pull Purines Derivatives: Toward the Development of New Photoluminescence Bioprobes"

Cocca, L. H. Z.; Abegao, L. M. G.; Sciuti, L. F.; Vabre, R.; **Siqueira, J. de P.*;** Kamada, K.; Mendonca, C. R.; Piguel, S.; De Boni, L.

Fluorescent organic molecules have received great attention due to their largest applications, for example, in DNA and RNA spectroscopies studies, development of new photoluminescence bioprobes, and applications in fluorescence spectroscopy. In specific, purine base analog molecules present high fluorescence quantum yields and significant Stokes shift. Furthermore, the addition of push-pull structures at the purine core could increase the photoluminescence properties, making candidates for photoluminescence bioprobes. To consider this, a complete spectroscopic study was performed on nine push-pull purines, distinguished by different push-pull structures. In specific, for this research, the two-photon absorption (2PA) study showed that the compounds present induced two-photon fluorescence at the therapeutic window, desired for fluorescence microscopy. The brightness property was evaluated, indicating that all chromospheres are fluorescent by a 2PA process. Additionally, ultrafast transient absorption was performed to elucidate contribution of the excited states on the 2PA spectra, and quantum chemistry calculations were performed to corroborate the experimental results.

JOURNAL OF PHYSICAL CHEMISTRY C 124[23], 12617-12627, 2020. DOI: 10.1021/acs.jpcc.0c01859

[P225-2020] "Ultra-simplified Single-Step Fabrication of Microstructured Optical Fiber"

Cordeiro, C. M. B.*; Ng, A. K. L.; Heidepriem, H. E.

Manufacturing optical fibers with a microstructured cross--section relies on the production of a fiber preform in a multiple-stage procedure, and drawing of the preform to fiber. These processes encompass the use of several dedicated and sophisticated equipment, including a fiber drawing tower. Here we demonstrate the use of a commercial table-top low-cost filament extruder to produce optical fibers with complex microstructure in a single step - from the pellets of the optical material directly to the final fiber.

The process does not include the use of an optical fiber drawing tower and is time, electrical power, and floor space efficient. Different fiber geometries (hexagonal-lattice solid core, suspended core and hollow core) were successfully fabricated and their geometries evaluated. Air guidance in a wavelength range where the fiber material is opaque was shown in the hollow core fiber.

SCIENTIFIC REPORTS 10[1], 9678, 2020. DOI: 10.1038/s41598-020-66632-3

Eventos publicados

[P226-2020] "Exploring fabrication methods to highly sensitive and selective InP nanowire biosensors"

Zavarize, M.*; Martins, M. N.*; von Zuben, A. A. G.*; Koledov, V.; von Gratowski, S.; **Cotta, M. A.***

Fabrication methodologies for integration of nano-objects into microscale devices is still an active area of research. Here we analyze possible methods of incorporation of semiconductor nanowires into lithographically-defined electrode pads. Mechanically-transferred InP nanowires were metallized into Au and Pt pads using a electron-beam-induced Pt metallization. Atomic and Kelvin Probe Force Microscopies show that a contamination of Pt on the nanowire and the region around it can prevent application of this technique to biosensors in which surface functionalization protocols must be applied as part of the fabrication methodology. Other transfer methods with more controlled nanowire positioning, such as nanotweezers, may be necessary to overcome this problem.

4th International Conference on Metamaterials and Nanophotonics (METANANO), St. Petersburg, RUSSIA. JUL 15-19, 2019.

Journal of Physics Conference Series 1461, 012003, 2020. DOI: 10.1088/1742-6596/1461/1/012003

Biografia

[B001-2020] "ANNA CAROLINA KREBS PEREIRA REGNER (1947-2020)"

Martins, R. de A.*; Silva, C. C.; Prestes, M. E. B.

ISIS 111[2], 362-364, 2020. DOI: 10.1086/709410

Correção

[Co02-2020] "Study of dijet events with a large rapidity gap between the two leading jets in pp collisions at root s = 7TeV (vol 78, 242, 2018)"

Sirunyan, A. M.; Tumasyan, A.; Adam, W.; **Chinellato, J. A.*; Tonelli Manganote, E. J.***; et. al.; CMS Collaboration

Events with no charged particles produced between the two leading jets are studied in proton-proton collisions at s√=7 TeV. The jets were required to have transverse momentum pjetT>40 GeV and pseudorapidity 1.5<|ηjet|<4.7, and to have values of ηjet with opposite signs. The data used for this study were collected with the CMS detector during low-luminosity running at the LHC, and correspond to an integrated luminosity of 8pb−1. Events with no charged particles with pT>0.2 GeV in the interval −1<η<1 between the jets are observed in excess of calculations that assume no color-singlet exchange. The fraction of events with such a rapidity gap, amounting to 0.5–1% of the selected dijet sample, is measured as a function of the pT of the second-leading jet and of the rapidity separation between the jets. The data are compared to previous measurements at the Tevatron, and to perturbative quantum chromodynamics calculations based on the Balitsky–Fadin–Kuraev–Lipatov evolution equations, including different models of the non-perturbative gap survival probability.

EUROPEAN PHYSICAL JOURNAL C 80[5], 441, 2020. DOI: 10.1140/epjc/s10052-020-7946-2

Errata Boletim Junho

(n. 3, Junho 20, P092-2020: artigo foi destaque de capa)

[P092-2020] "Computed tomography-based skeletal segmentation for quantitative PET metrics of bone involvement in multiple myeloma" (Artigo destaque de capa)

Takahashi, M. E. S.*; Mosci, C.; Souza, E. M.; Brunetto, S. Q.; de Souza, C.; Pericole, F. V.; Lorand-Metze, I.; Ramos, C. D.

Purpose: Quantifications in nuclear medicine are occasionally limited by the lack of standardization for defining volumes of interest (VOIs) on functional images. In the present article, we propose the use of computed tomography (CT)-based skeletal segmentation to determine anatomically the VOI in order to calculate quantitative parameters of fluorine 18 fluorodeoxyglucose (F-18-FDG) PET/CT images from patients with multiple myeloma. Methods: We evaluated 101 whole-body F-18-FDG PET/CTs of 58 patients with multiple myeloma. An initial subjective visual analysis of the PET images was used to classify the bone involvement as negative/mild, moderate, or marked. Then, a fully automated CT-based segmentation of the skeleton was performed on PET images. The maximum, mean, and SD of the standardized uptake values (SUVmax, SUVmean, and SDSUV) were calculated for bone tissue and compared with the visual analysis. Results: Forty-five (44.5%), 32 (31.7%), and 24 (23.8%) PET images were, respectively, classified as negative/mild, moderate, or marked bone involvement. All quantitative parameters were significantly related to the visual assessment of bone involvement. This association was stronger for the SUVmean [odds ratio (OR): 10.52 (95% confidence interval (CI), 5.68-19.48); P < 0.0001] and for the SDSUV [OR: 5.58 (95% CI, 3.31-9.42); P < 0.001) than for the SUVmax [OR: 1.01 (95% CI, 1.003-1.022); P = 0.003]. Conclusion: CT-based skeletal segmentation allows for automated and therefore reproducible calculation of PET quantitative parameters of bone involvement in patients with multiple myeloma. Using this method, the SUVmean and its respective SD correlated better with the visual analysis of F-18-FDG PET images than SUVmax. Its value in staging and evaluating therapy response needs to be evaluated.

NUCLEAR MEDICINE COMMUNICATIONS 41[4], 377-382, 2020. DOI: 10.1097/MNM.0000000000001165

***autores da comunidade IFGW.**
Fonte: Web of Science

Defesas de Dissertações do IFGW

[D011-2020] "Anéis microrressonadores acoplados em plataforma de silício como fonte de atraso e avanço de sinais ópticos"
Aluno: Michel Benite Rossi
Orientador: Prof. Dr. Newton Cesário Frateschi
Data: 20/07/2020

[D012-2020] "Estudo AB-initio de intermetálicos de Zr-Fe e seus hidretos"
Aluno: Bárbara Maria Teixeira Costa Peluzo
Orientador: Prof. Dr. Silvio Antonio Sachetto Vitiello
Data: 21/07/2020

[D013-2020] "Análise computacional de ondas dispersivas em poços preenchidos por fluidos"
Aluno: Diego Salam Claro
Orientador: Prof. Dr. Odilon Divino Damasceno Couto Junior
Data: 31/08/2020

Defesas de Teses do IFGW

[T008-2020] "Defeitos Pontuais Em Um Sólido Quântico"
Aluno: Vitor Zamprônio Pedroso
Orientador: Prof. Dr. Silvio Antonio Sachetto Vitiello
Data: 28/07/2020

[T009-2020] "Aspectos da geração de massa dinâmica dentro do formalismo das Equações de Schwinger-Dyson"
Aluno: Clara Teixeira Figueiredo
Orientador: Profa. Dra. Arlene Cristina Aguilar
Data: 20/08/2020

[T010-2020] "Simulando colisões de íons pesados usando um modelo híbrido baseado em QCD e espalhamento hadrônico"
Aluno: André Vieira da Silva
Orientador: Prof. Dr. David Dobrigkeit Chinellato
Data: 27/08/2020

Fonte: Portal IFGW/Pós-graduação - Agenda de Colóquios, Defesas e Seminários.
Disponível em: http://portal.ifi.unicamp.br/pos-graduacao

Observação:
Não ocorreram neste período defesas de teses e dissertações do PECIM com orientadores do IFGW.

Fonte: Página do PECIM - Programa de Pós-Graduação Multiunidades em Ensino de Ciências e Matemática - Mestrado e Doutorado (PECIM) da Unicamp.
Disponível em: https://www.pecim.unicamp.br/bancas

Abstracta

Instituto de Física
Diretor: Prof. Dr. Pascoal José Giglio Pagliuso
Diretora Associada: Profa. Dra. Mônica Alonso Cotta
Universidade Estadual de Campinas - UNICAMP
Cidade Universitária Zeferino Vaz
13083-859 - Campinas - SP - Brasil
e-mail: secdir@ifi.unicamp.br
Fone: +55 19 3521-5300

Publicação

Biblioteca do Instituto de Física Gleb Wataghin
http://portal.ifi.unicamp.br/biblioteca

Diretora Técnica: Sandra Maria Carlos Cartaxo
Coordenadora da Comissão de Biblioteca: Profa. Dra. Arlene Cristina Aguilar

Elaboração:
Maria Graciele Trevisan (Bibliotecária)
Ayres Neri da Cunha Junior (Técnico Administrativo)
contato: infobif@ifi.unicamp.br